Chuanjin Su
Department of Mechanical and Aerospace Engineering,
University of California, Los Angeles,
Los Angeles, CA 90095

Huan Wu
Department of Mechanical and Aerospace Engineering,
University of California, Los Angeles,
Los Angeles, CA 90095

Lingyun Dai
Department of Mechanical and Aerospace Engineering,
University of California, Los Angeles,
Los Angeles, CA 90095

Zhihan Zhang
Department of Mechanical and Aerospace Engineering,
University of California, Los Angeles,
Los Angeles, CA 90095

Suixuan Li
Department of Mechanical and Aerospace Engineering,
University of California, Los Angeles,
Los Angeles, CA 90095

Yongjie Hu[1]
Department of Mechanical and Aerospace Engineering,
University of California, Los Angeles,
Los Angeles, CA 90095
e-mail: yhu@seas.ucla.edu

Nonclassical Heat Transfer and Recent Progress

Heat transfer in solids has traditionally been described by Fourier's law, which assumes local equilibrium and a diffusive transport regime. However, advancements in nanotechnology and the development of novel materials have revealed nonclassical heat transfer phenomena that extend beyond this traditional framework. These phenomena, which can be broadly categorized into those governed by kinetic theory and those extending beyond it, include ballistic transport, phonon hydrodynamics, coherent phonon transport, Anderson localization, and glass-like heat transfer. Recent theoretical and experimental studies have focused on characterizing these nonclassical behaviors using methods such as the Boltzmann transport equation, molecular dynamics, and advanced spectroscopy techniques. In particular, the dual nature of phonons, exhibiting both particle-like and wave-like characteristics, is fundamental to understanding these phenomena. This review summarizes state-of-the-art findings in the field, highlighting the importance of integrating both particle and wave models to fully capture the complexities of heat transfer in modern materials. The emergence of new research areas, such as chiral and topological phonons, further underscores the potential for advancing phonon engineering. These developments open up exciting opportunities for designing materials with tailored thermal properties and new device mechanisms, potentially leading to applications in thermal management, energy technologies, and quantum science. [DOI: 10.1115/1.4066973]

1 Introduction

For over two centuries, Fourier's law has been the foundational theory of heat conduction, traditionally describing heat flux as proportional to the temperature gradient. Despite its general success, Joseph Fourier initially based the law on the assumptions of local equilibrium and a linear response, without accounting for the underlying mechanisms [1]. In modern terms, these assumptions align with the diffusive heat transfer regime, where heat carriers, such as phonons in nonmetallic solids, undergo random walks, resulting in a mean free path (MFP) that is small relative to the system size. While the introduction of concepts like heat carriers and phonon MFP has somewhat limited the applicability of Fourier's law, diffusive heat transfer still prevails in most materials and

devices, allowing Fourier's law to remain applicable in many practical situations [2].

However, the rapid advancement of nanotechnology [3], new materials, devices, and extreme conditions [4–6] have unveiled heat transfer phenomena that extend beyond the traditional diffusive regime, necessitating a deeper understanding to advance thermal management and energy technologies. These nonclassical heat transfer phenomena can be broadly categorized into two types: those governed by kinetic theory and those extending beyond it. The first category includes phenomena such as ballistic transport, phonon hydrodynamics, and near-surface or interfacial thermal transport, which can be described using kinetic models like the Boltzmann Transport Equation (BTE) [7,8]. The second category encompasses effects that rely on the wave-like nature of lattice vibrations, requiring alternative approaches such as the Wigner formulation of the transport equation [9,10].

In Fig. 1, we outline several regimes of nonclassical heat transfer, characterized by two key parameters: the phonon MFP (Λ), which

represents the distance a phonon travels between successive scatterings, and the coherent length (ξ), indicates the distance over which phase coherence of lattice waves is preserved. Classical heat transfer occurs in the diffusive regime, where both Λ and ξ are significantly shorter than the characteristic length (L), but longer than the phonon wavelength (λ), ensuring that heat transfer is dominated by orthogonal vibrational modes, validating the particle-like behavior of the phonon gas. In this regime, sufficient phonon scatterings maintain local thermal equilibrium, allowing heat to be transported via diffusion. However, when L is reduced to a scale comparable to or smaller than Λ, the number of phonon scatterings becomes insufficient for diffusive transport, leading to ballistic heat transfer, where phonons propagate without scattering, akin to radiation. Hydrodynamic phonon transport can occur when momentum-conserving scatterings dominate over momentum-destroying ones and L is between the MFPs of these two types of scatterings, resulting in fluid-like heat transfer behaviors, analogous to viscosity and convection. The hydrodynamic, ballistic and diffusive phonon transport could coexist due to the broad range of spectral-dependent phonon MFP. When ξ becomes comparable to or exceeds L, phase coherence can be preserved over long distances, leading to a different heat transfer mechanism known as coherent phonon transport. This phenomenon can occur in superlattices, where the characteristic length L refers to the period thickness. In certain systems where Λ is short due to numerous phase-preserving scatterings but coherence length ξ is sufficiently long, constructive and destructive interference effects can enhance or hinder phonon transport in specific regions, potentially leading to strongly localized vibrational modes, a phenomenon known as Anderson localization. Conversely, when Λ or ξ becomes shorter than λ, lattice waves lose phase coherence, resulting in localized vibrational modes that transport through wave-like tunneling processes. This regime is typically observed in disordered or strongly anharmonic systems, exhibiting heat transfer behavior similar to that of glasses. These nonclassical heat transfer phenomena have garnered significant interest in recent years, presenting both new challenges and opportunities to advance our understanding of heat transfer.

Recent efforts from both theoretical and experimental perspectives have sought to understand and characterize these nonclassical heat transfer phenomena. Theoretical studies employ methods such as lattice dynamics (LD) [11–19], Monte Carlo (MC) method [20–26], molecular dynamics (MD) [27–31], and the atomistic Green's 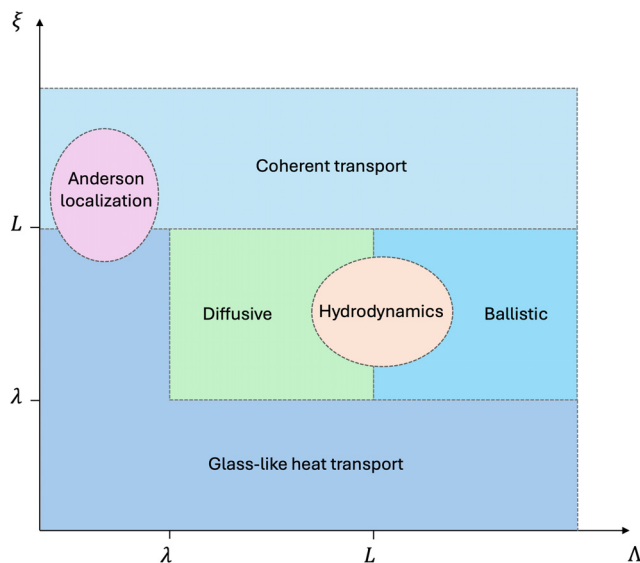function (AGF) [32]. These approaches are used to characterize the thermal properties of materials and interfaces and to elucidate the underlying heat transfer processes. LD provides direct solutions to phonon theory, yielding both harmonic and anharmonic properties of materials, such as phonon dispersion, phonon density of states (DOS), and phonon lifetimes. Based on LD results, the phonon BTE can be numerically solved by MC method that randomly samples phonon bundles to characterize heat transport processes. MD simulations, grounded in classical mechanics, utilize interatomic potentials to extract valuable information from the dynamic trajectories of atoms. AGF uses harmonic matrices of contacts and devices to solve the transmission coefficient across structures, studying heat transport across interfaces and within nanostructures. Collectively, these theoretical methods cover a wide range of length and time scales, offering deep insights into heat transport mechanisms and aiding in the design of materials with tailored thermal properties. On the experimental front, advanced techniques [33] have been developed to enhance the understanding of nondiffusive heat transfer, including pump-probe spectroscopy methods, such as time-domain thermoreflectance (TDTR) [34–37], frequency-domain thermoreflectance (FDTR) [38], and transient thermal grating [39] methods, as well as nanoscale thermometries [40]. These experimental approaches enable precise measurement of thermal properties, including thermal conductivity, thermal boundary resistance (TBR), vibrational modes, phonon MFPs, and phonon lifetimes, with high accuracy and resolution. By integrating theoretical and experimental studies, nonclassical heat transfer has been extensively explored across various materials and systems, including bulk materials, thin films, nanostructures, and interfaces. This comprehensive investigation has led to the discovery of new phenomena and the development of innovative materials and devices.

The rest of this review is organized as follows: Following Fig. 1, ballistic regime, phonon hydrodynamics, glass-like heat transport, and coherent heat transport will be discussed in Secs. 2–5, respectively. Expanding our scope of nonclassical heat transfer, recent studies on interfacial heat transport, near-field radiation, and surface phonon polariton will be covered in Secs. 6–8. Finally, in Sec. 9, we conclude the review and introduce future outlooks, summarizing the key findings and discussing potential directions for further research.

2 Ballistic Heat Transfer

In the microscopic picture of heat transfer in solids, where phonons are the dominant heat carriers, thermal transport is governed by the phonon BTE [8], originally introduced by Peierls [7] as follows:

$$\frac{\partial n}{\partial t} + \mathbf{v}_{g,\mathbf{q}s} \cdot \nabla n = \left(\frac{\partial n}{\partial t}\right)_{\text{scatt}}$$

where n is the phonon distribution function that gives the density of phonons at position $\mathbf{x}$ in mode $\mathbf{q}s$, and $\mathbf{v}_{g,\mathbf{q}s}$ is the group velocity. Here, $\mathbf{q}$ marks wavevector and s is the branch index. To characterize the scattering term on the right-hand side of the phonon BTE, the relaxation time approximation (RTA) is often employed, utilizing the Bhatnagar-Gross-Krook operator [41], is often employed. This approach assumes that the phonon distribution function relaxes to the equilibrium distribution function n_0 with a relaxation time $\tau_{\mathbf{q}s}$. Under this approximation, the BTE can be solved by assuming that n is close to n_0 and the difference between them, $\delta n_{\mathbf{q}s} = n_{\mathbf{q}s} - n_{0,\mathbf{q}s}$, has no spatial and temperature variations. The difference is given by $\delta n_{\mathbf{q}s} = -\tau_{\mathbf{q}s}(\partial n_{0,\mathbf{q}s}/\partial T)v_g \cdot \nabla T$. The thermal conductivity tensor for a bulk material is then expressed as

$$\kappa_{ij} = \left\langle c_{\mathbf{q}s} v_{g,\mathbf{q}s,i} v_{g,\mathbf{q}s,j} \tau_{\mathbf{q}s}\right\rangle_{\text{BZ}}$$

where $\langle \cdot \rangle_{\text{BZ}}$ denotes integration over the first Brillouin zone and summation over phonon branches, $C_{\mathbf{q}s}$ is the volumetric specific heat of mode $\mathbf{q}s$. In an isotropic manner, the thermal conductivity can be

Fig. 1 Regimes of heat conduction characterized by the phonon mean free path (Λ) and phonon coherence length (ξ), in comparison with the phonon wavelength (λ) and characteristic size (L)
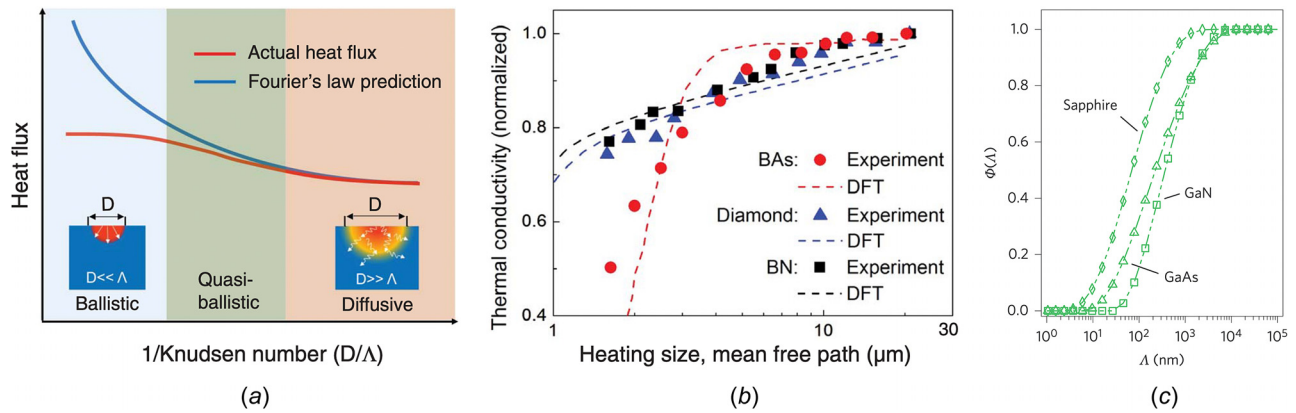
Fig. 2 Ballistic heat transfer. (*a*, *b*) Adapted from *Science* 361, 575, 2018. (*a*) Schematic of heat flux for a fixed temperature difference as a function of the Knudsen number. Red and blue lines indicate the actual heat flux and the flux predicted by Fourier's law, respectively. Insets show that the thermal transport evolves from a diffusive to a ballistic regime when the heating size is gradually reduced. When the actual heat flux was measured and fitted to Fourier's law to obtain an effective thermal conductivity (k_{eff}), a gradual reduction in k_{eff} was expected with a decreasing heating size. Essentially, the k_{eff} decrease is due to the evolution from diffusive to ballistic transport for the phonons with a mean free path comparable to the heating size, and thereby represents the phonon MFP spectra. (*b*) Effective thermal conductivity was measured for the three best thermal conductors (BAs, diamond, and BN), as a function of heating diameters from 21 to 1.6 μm. Experimental results, compared with the MFP spectra calculated with DFT, indicate that in BAs, a large portion of phonons have long mean free paths, owing to the distinctive band structure of BAs. (*c*) Reconstruction of phonon MFP contributions to the thermal conductivities for sapphire, GaAs and GaN. Adapted from *Nat. Nanotechnol.* 10, 701–706, 2015.

simplified as $\kappa = \frac{1}{3} \langle c_{qs} v_{g,qs} \Lambda_{qs} \rangle_{BZ}$, where $\Lambda_{qs} = v_{g,qs} \tau_{qs}$ represents the phonon MFP.

However, this derivation is only valid when the phonon MFP is much smaller than the system size, a condition under which the bulk assumption holds. When the phonon MFP is comparable to or even larger than the system size, the ballistic heat transfer regime emerges (Fig. 2(*a*)), where phonons can travel without scattering, making boundary scattering more significant. At small scales or low temperatures, a reduced thermal conductivity can be expected, as the intrinsic phonon MFP is constrained by the system size. Casimir [42] first proposed the proportionality between the thermal conductivity and the system size, a concept now known as the Casimir limit. Using equilibrium MD, Henry and Chen [27] estimated that at room temperature, phonons with MFPs larger than 1 μm contribute 35% of the total thermal conductivity of silicon. Based on Landauer formalism, Jeong et al. [43] showed that both the in-plane and cross-plane thermal conductivities of silicon thin films are reduced due to the boundary scattering. With advances in computational power, ab initio calculations have become feasible for studying heat transfer [44]. By extracting force constants from density functional theory (DFT) calculations, Broido, Mingo, Lindsay et al. employed the perturbation theory to calculate the mode-dependent phonon scattering time [13–16,18,19,45–48]. Esfarjani and Chen [13] calculated the accumulative thermal conductivity of silicon as a function of phonon MFP.

In addition to the reduced thermal conductivity, temperature jumps at boundaries were explored in various theoretical studies. Klitsner et al. [49] proposed the temperature jumps by studying the concept of phonon radiative transport, and this phenomenon was further explored by Joshi and Majumdar [50] through solving the equation of phonon radiative transport [51]. Chen [52] attributed this temperature jump to the nonequilibrium nature of the transport process and the energy-based definition of temperature. Maassen and Lundstrom [53,54] used McKelvey-Shockley flux method to derive a simplified phonon BTE to capture the boundary temperature jump attributed to the ballistic thermal resistance. They found that this resistance is an intrinsic material property rooted in the nonequilibrium nature of phonon ballistic transport, rather than being a result of enhanced phonon scattering at the contacts.

Taking ballistic effects into account, several efforts have been made to modify Fourier's law. Chen [55,56] proposed a ballistic-diffusive model that separates the diffusive component within the

material from the ballistic component associated with boundaries. By attributing the ballistic effects to the boundaries, the ballistic-diffusive model shows better agreement with the phonon BTE than the Cattaneo-Vernotte (CV) model [57,58], even though the mathematical form of the ballistic component in the ballistic-diffusive model is identical to that in the CV model. Alvarez and Jou [59] included Knudsen number dependent thermal conductivity in the hyperbolic formulation of the Fourier's law without separating the ballistic and diffusive components, finding results similar to those of Chen's model [55,56].

In recent years, ab initio approaches for phonon calculations at the nanoscale have advanced significantly, and various high-efficiency software packages have become widely available. Popular DFT software includes VASP [60,61], Quantum ESPRESSO (QE) [62–64], CP2K [65], ABINIT [66], and OpenMX [67]. Harmonic properties, such as phonon dispersion, DOS, and heat capacity, can be computed either using built-in DFPT codes in VASP, QE, and ABINIT, or by applying the finite displacement method in combination with one of the DFT software packages and phonon calculation tools like ALAMODE [68], Phonopy [69,70], and ShengBTE [71] and the FourPhonon [72] module. The finite displacement method is also widely used for determining anharmonic force constants and calculating phonon scattering. The direct solution of the phonon BTE has also advanced, with approaches categorized into stochastic and deterministic methods [73]. Stochastic methods are primarily based on MC sampling, including phonon-tracing MC [22,74–76], which traces the generation and scattering of one phonon bundle at a time, and ensemble MC [25,26], which handles all sampled phonons simultaneously. Phonon-tracing MC is typically based on the RTA and is more efficient with the energy-based variation-reduced formulation [22,74], while ensemble MC is capable of handling the full scattering matrix formulation. Deterministic solutions include the finite volume method [77,78], the discrete ordinates method [79–81] originally used to solve the radiative heat transfer equation, and the discrete unified gas kinetic scheme [82]. However, due to the high dimensionality of the phonon BTE, deterministic solutions are usually limited to the RTA, as discretizing the phonon BTE with more complex scattering terms requires large computational resources. Efforts have also been made to unify the phonon BTE and nonequilibrium MD (NEMD) at the mode level [83–86] to reduce the computational resources demanded by NEMD and to study the modal nonequilibrium of phonons.

On the experimental side, early work focused on measuring the effects of sample size due to quasi-ballistic transport and boundary scattering. Asheghi et al. [87,88], measured thermal conductivity reduction in silicon thin films from the bulk value. Johnson and Cuffe et al. [89] studied in-plane thermal transport in silicon membranes with varying thermal grating periods. Minnich [90] measured reduced thermal conductivity in bulk silicon when the heating area was minimized using laser spot sizes. To establish more quantitative relationships between size-dependent measurements and phonon spectra, Dames and Chen developed a method to project cumulative thermal conductivity into phonon MFP distributions [91,92]. Minnich et al. [90] introduced a suppression function to relate phonon MFP to thermal length. A direct measurement and comprehensive reconstruction of phonon spectral contributions to thermal conductivity were achieved by Hu, Zeng, and Chen et al. [23,93], spanning a heating range from 30 nm to 100 μm. They constructed phonon MFP spectra for several technologically important materials, including Si, GaN, and GaAs from experiments (Fig. 2(c)), in consistency with ab initio modeling based on transient, frequency-dependent BTE and multiscale Monte Carlo methods. These progresses developed new methodologies and provided quantitative understanding of confinement effects on phonon scattering that deviate from Fourier's law.

3 Phonon Hydrodynamics

Phonon hydrodynamic transport refers to a distinct regime of heat transfer in solids where phonons exhibit collective, fluid-like behavior, akin to particles in a fluid. This regime arises under specific conditions where phonon-phonon scattering is predominantly governed by normal (N) processes, which conserve crystal momentum, rather than Umklapp (U) processes, which do not. Phonon-phonon scattering can be categorized into these two processes (Fig. 3(a)): normal processes conserve crystal momentum, while Umklapp processes do not. At cryogenic temperatures, the population of phonons with large wavevectors (typically associated with high energy) is suppressed, leading to a reduction in Umklapp processes and allowing normal processes to dominate. Due to the conservation of crystal momentum in normal processes, phonons in this regime exhibit fluid-like behavior, drawing an analogy between the phonon gas and the particle description of fluid flows. This collective behavior of phonons is referred to as phonon hydrodynamics. The investigations of phonon hydrodynamic effects can be traced back to the observations of the second sound in superfluid helium [94] and then in solid helium [95], NaF crystal [96,97], and Bi crystal [98]. As shown in Fig. 3(d), when heat pulses are applied to one end of the sample, the signal detected at the other end indicates that heat propagates as a wave rather than diffusing through the sample [99]. Different from the first sound, which involves the propagation of pressure waves through a material, the second sound is the result of the propagation of waves formed by collectively excited phonons. Early studies on phonon hydrodynamics treats phonon gas as a fluid and solving the Navier–Stokes equation [100,101]. Later, more accurate phonon hydrodynamic equations were derived from the phonon BTE, providing a more precise description of heat propagation and phonon dynamics in materials [101,102].

However, due to the complexity of describing and solving phonon scattering in the phonon BTE, the phonon hydrodynamics was mainly described by phenomenological models [103] until recent years when directly solving the phonon BTE in a beyond-RTA manner becomes feasible. Since the normal processes merely redistribute phonon momentum among different modes, and no thermal resistance is induced, RTA treatment for the scattering term in the phonon BTE that does not distinguish between normal and Umklapp processes cannot capture the phonon hydrodynamics, hence underestimates the lattice thermal conductivity [104–106]. To overcome this limitation, Callaway [104] modified the scattering term by separating the normal and Umklapp processes

$$\left(\frac{\partial n}{\partial t}\right)_{\text{scatt}} = -\frac{n - n_0}{\tau_{qs,\text{U}}} - \frac{n - n_{\text{d}}}{\tau_{qs,\text{N}}}$$

where Umklapp and normal processes are considered to redistribute phonon population to equilibrium distribution n_0 and displaced distribution n_{d}, respectively. The lattice thermal conductivity estimated using Callaway's approximation for phonon scattering effectively captures phonon hydrodynamics in materials with strong normal scattering processes [107,108]. The phonon hydrodynamics at nanoscale was simulated in two-dimensional (2D) materials by solving BTE under Callaway's approximation using discrete ordinates method [80]. However, a more accurate description on phonon hydrodynamics requires a comprehensive consideration of the scattering matrix, which reformulates the phonon scattering term as

$$\left(\frac{\partial n_{qs}}{\partial t}\right)_{\text{scatt}} = -\sum_{q's'}\Omega_{qs,q's'}\left(n_{q's'} - n_{q's'}^0\right)$$

where $\Omega_{qs,q's'}$ is the scattering matrix that represent the transition rate from mode $q's'$ to qs. Iterative approaches have been employed to solve the BTE with the full scattering matrix, yielding an exact solution for lattice thermal conductivity that incorporates ab initio methods based on DFT. The thermal conductivity of graphite is one order of magnitude higher when accurately accounting for phonon hydrodynamics, demonstrating the significant collective excitations in graphite due to strong normal processes [109]. Lee and Chen solve the BTE for hydrodynamic phonon transport in suspended graphene using Green's function approach [99]. Besides, the BTE with full
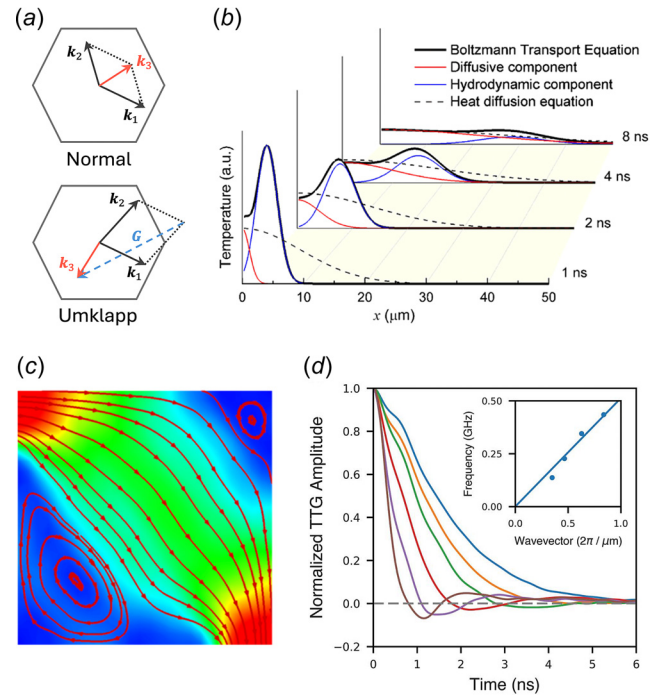

Fig. 3 Hydrodynamic thermal transport. (*a*) Schematic of normal scattering and Umklapp scattering. (*b, c*) Adapted from *Int. J. Heat Mass Transfer* 220, 124988, 2024. (*b*) Temperature field response to a heat pulse under a background temperature of 100 K. The temperature field determined by the phonon BTE (black solid) shows noticeable difference from the Fourier's law (back dashed). (*c*) Phonon vortex predicted by the phonon BTE using full matrix scattering. (*d*) Second sound signal in graphite at 85 K for various grating periods. The inset shows the second sound frequency (circles) plotted against the wavevector, with a solid line representing a linear fit that corresponds to a phase velocity of 3200 m/s. Adapted from *Science* 364, 6438, 2019.

scattering matrix was further solved in real space using MC algorithm [25], enabling the simulation of hydrodynamic phonon transport in nanostructures. Through this MC simulation, steady-state hydrodynamic phonon transport in graphene ribbons was simulated, showing an analogy to Poiseuille flow in fluids, and thermal viscosity was identified [110]. The phonon hydrodynamic equations with the viscous term were derived from the BTE with full scattering matrix [111], where the thermal viscosity stems from phonon interactions and can be derived from the eigenvectors of the scattering matrix. By solving the BTE with full scattering matrix using MC algorithm, Wu and Hu [26] simulated the propagation dynamics of the hydrodynamic waves (Fig. 3(b)) and reported fluid-like behaviors of phonons such as vortex and jet flow (Fig. 3(c)) in graphite.

Experimental study of phonon hydrodynamics was generally limited to the low-temperature regime until recent theoretical predictions that strong phonon hydrodynamics can exist in a group of two-dimensional materials including graphene and h-BN [112,113]. Huberman et al. [99] observed the existence of second sound in graphite between 85 K and 125 K, confirming the ab initio calculations. More recently, Ding and Chen et al [114] further measured the second sound at around 200 K using improved transient grating technique. At higher temperature, the experimental studies are still rudimentary. Machida et al. [115] claimed that the room-temperature in-plane thermal conductivity of graphite can be enhanced with decreasing thickness, which was attributed to the existence of phonon hydrodynamics.

4 Glass-Like Heat Transfer

Besides the particle-like behavior of phonons that can be formulated by the kinetic theory [7,8], the dual quantum nature of phonons also allows them to exhibit their wave nature, especially in glass-like heat transfer. The phonons are quantized lattice waves, hence inherent with wave nature. In most crystals, the coherent lengths of the lattice waves are much longer than their wavelengths, allowing for the quantization of lattice waves and the treatment of phonons as particles, as shown in Fig. 4(a). However, when the coherent length is shorter or comparable with the wavelength, the vibrational modes are localized and transport through a wave-like tunneling process. Such wave-like tunneling process usually happens to amorphous due to the reduced coherence by disorder.

The early attempt to treat the phonon localization was made by Allen and Feldman [116] (AF) when studying disordered materials. In the AF theory treatment, a heat current operator S is proposed, based on which the concept of mode diffusivity D_i for mode i is introduced by reformulating the Green-Kubo formula within in the framework of harmonic approximations [117,118]. The mode diffusivity evaluates the coupling between local vibrational modes, representing the participation of mode i in the heat transport, and the sum of all mode diffusivities times the specific heat gives the thermal conductivity. Since its introduction, the AF theory combining with the particle-like behavior of phonons has been widely used to study disordered materials such as amorphous materials [116,119–123] and complex crystals [124]. However, the applicability of the AF theory is limited due to its exclusion of the anharmonicity. Shenogin et al. [125] Compared the thermal conductivity of amorphous silicon obtained by the AF theory with the results from MD simulations, and found that the AF theory overestimates the thermal conductivity for systems with complex compositions in which the anharmonicity plays a significant role.

In addition, though most of the vibrational modes in disordered materials are localized or quasi-localized, it is also possible that some low-frequency modes have long MFP and significantly contribute to heat transport. Allen et al. [120] categorized vibrational modes into propagons, diffons and locons by their properties of propagation or localization, and treated the propagons as phonon-like modes that have relatively larger MFP. However, since only off-diagonal elements are considered, the heat current contributed by the propagation of coherent lattice waves (phonons) are excluded [9], thus, the contribution of propagons cannot be taken into account by the original AF theory. Through examining amorphous silicon, Allen et al. [119] concluded that only about
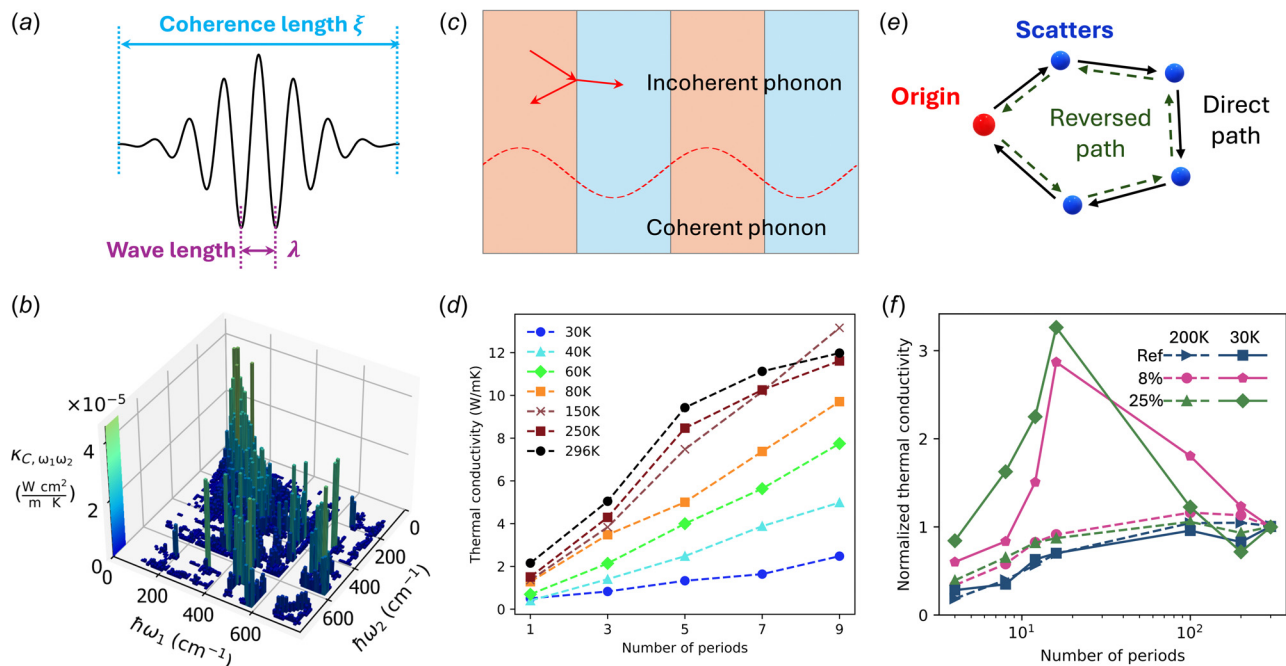

Fig. 4 Coherent phonon transport and Anderson localization. (*a*) Schematic of wavelength and coherence length. (*b*) Two-dimensional DoS for the thermal conductivity of $La_2Zr_2O_7$ at 1300 K, revealing the coupling between two vibrational modes. Adapted from *Phys. Rev. X* 12, 041011, 2022. (*c*) Schematic of incoherent and coherent phonon transport in superlattices. (*d*) Thermal conductivity of GaAs/AlAs superlattices with fixed period thickness. The increasing trend indicates ballistic transport across superlattices, demonstrating the existence of coherent transport. Adapted from *Science* 338, 6109, 2012. (*e*) Schematic of Anderson localization. (*f*) Normalized Thermal conductivity of GaAs/AlAs superlattices with ErAs nanodots inserted at interfaces. The decreasing trend with respect to the number of periods is due to Anderson localization. Adapted from *Science* 4, 12, 2018.

4% vibrational modes are propagons. However, recent MD calculations [121,126] found that propagons of amorphous silicon can significantly contribute up to half of the total thermal conductivity despite the small populations. The role of propagons is also confirmed by experimental studies on the thickness-dependency of the thermal conductivity [127] and the MFP spectra [128]. The lattice thermal conductivity contributed by propagative modes and nonpropagative modes was estimated by a two-channel model and compared with experiments, showing non-negligible contribution from nonpropagative modes in crystal materials with strong anharmonicity [129].

To improve the AF theory, efforts bridging heat transport in crystalline and amorphous have been made by Isaeva et al. [130] through an improved quasi-harmonic approach to the reformulation of the Green-Kubo formula. It is found that the approach is robust when dealing with systems with any kinds of structural order. A more rigorous treatment is established by Simoncelli et al. [9,10] through the Wigner formulation of the transport equation

$$
\begin{aligned}
&\frac{\partial}{\partial t} n(\boldsymbol{x}, \boldsymbol{q}, t)_{s,s'} + i\left[\omega(\boldsymbol{q})_s n(\boldsymbol{x}, \boldsymbol{q}, t)_{s,s'} - n(\boldsymbol{x}, \boldsymbol{q}, t)_{s,s'} \omega(\boldsymbol{q})_{s'}\right] \\
&+ \frac{1}{2}\left\{\sum_{s''} \boldsymbol{v}(\boldsymbol{q})_{s,s''} \cdot \nabla_{\boldsymbol{x}} n(\boldsymbol{x}, \boldsymbol{q}, t)_{s'',s'}\right. \\
&\left.+ \sum_{s''} \nabla_{\boldsymbol{x}} n(\boldsymbol{x}, \boldsymbol{q}, t)_{s,s''} \cdot \boldsymbol{v}(\boldsymbol{q})_{s'',s'}\right\} = \left.\frac{\partial n(\boldsymbol{x}, \boldsymbol{q}, t)_{s,s'}}{\partial t}\right|_{\hat{H}^{\mathrm{per}}}
\end{aligned}
$$

where $n(\boldsymbol{x}, \boldsymbol{q}, t)_{s,s'}$ and $\boldsymbol{v}(\boldsymbol{q})_{s,s'}$ are the generalization of the phonon distribution function and the group velocity, respectively. The diagonal terms represent the same physics as the phonon BTE formulation in the phonon BTE (population channel). The off-diagonal terms describe the wave-like tunneling behavior of localized modes, which are related to the phase coherence between pairs of eigenstates s and s' (coherence channel). It is found that the Wigner formulation can be reduced to both the phonon BTE and the AF theory under certain conditions, thus providing a unified framework to study the phonon transport in a wide range of scenarios. Applying this unified framework, the thermal conductivity of La$_2$Zr$_2$O$_7$ was calculated. Fig. 4(b) presents the diagonal and off-diagonal contributions to the La$_2$Zr$_2$O$_7$ thermal conductivity. It was found that phonon branches with large group velocities contribute more to the population channel, while the flat phonon branches contribute more to the coherence channel [9]. In addition to complex crystals, Simoncelli et al. [131] investigated the thermal conductivity of amorphous silicon oxide, and found agreement with both the experimental results and the prediction of the AF theory, validating the ab initio approach to studying heat transport in amorphous materials. These studies on advancing glass-like heat transport may facilitate future material applications such as thermoelectrics [132], thermal insulation [133], and sustainable building technologies [134].

5 Coherent Heat Transport

Phonon transport is usually modeled using particle-based methods as in the BTE, where the phase information of lattice waves is assumed to be unimportant and thus neglected. However, when multiple interfaces exist at the nanoscale in a periodic pattern, the particle picture could be insufficient for describing transport physics due to interference between forward and backscattered lattice waves; hence, the wave nature of the phonon must be considered. Typical examples include superlattices where two alternating layers of different materials with high-quality interfaces, consisting of a supercell whose period could be as small as a few angstroms. As shown in Fig. 4(c), when the period length is large, the heat transport is in diffusive regime, therefore a simple description based on particle models is valid. In this diffusive regime, as the period length becomes smaller, phonon MFPs reduce due to interface scatterings, leading to decreasing thermal conductivity. However, as the period decreases further to lengths comparable to or smaller than the phonon intrinsic anharmonic MFP, the reflected waves can retain their phase information over multiple periods before undergoing anharmonic scattering. The preservation of phase allows for (non-)constructive interference between waves, leading to the formation of a new folded phonon band structure with minibands and band gaps, thereby reshaping the modes available for transmission within the material [135]. These phonon modes, also known as coherent phonons in contrast to incoherent particle-like phonons, travel inside the material as if in a homogeneous medium where the interface does not serve as a scattering site and has MFPs greater than the period length. In these regimes, as the period reduces, the thermal conductivity goes up due to less band flattening caused by the reduced band-folding effect. Such a crossover between coherent and noncoherent transport regimes in thermal conductivity has been highlighted in both experimental and computational studies.

Extensive modeling efforts on coherent/incoherent phonon transport in superlattices are documented. Explorations start from particle methods: by assuming the phonon behaviors in neighboring layers are uncorrelated and interfaces scatter phonons, the solutions to the BTE [136,137] reveal an increasing thermal conductivity as the period length increases in GaAs/AlAs and Si/Ge superlattices. Pure wave models assume phonons are correlated in neighboring layers and require the use of supercell for phonon band calculation. Harmonic lattice dynamics on Si/Ge superlattices [138–140] predicts the decrease of thermal conductivity versus period length and attributed the finding to the reduced phonon velocity due to band gap opening. An imaginary component added to the phonon wavevector has been phenomenologically proposed to integrate the particle and wave pictures together [141], matching the experimental observation on nonmonotonic thermal conductivity behavior [142]. Later on, by combining first-principles DFT with the BTE method, the mode-wise group velocities, heat capacities, and scattering lifetimes of coherent phonon modes along with interface roughness effects in Si/Ge superlattices [143] have been thoroughly examined in superlattices. Greens function methods [144,145], though fully harmonic, have also been adopted to probe the spectral phonon transmittance through the superlattices.

Different than the aforementioned methods, which need to assume the coherent/incoherent nature of phonon modes, molecular dynamics, which rely on the atomic trajectories in real space, have no such prior assumptions, and thus can naturally include both the coherent and incoherent effects. The effect of interfacial species mixing on the thermal conductivity of Si/Si$_{0.7}$Ge$_{0.3}$ and Si/Ge has been studied using molecular dynamics [146]. A detailed computational study identified the relationship between heat transfer regime and phonon coherence length, MFPs, and superlattice period length [147]. Computations on relevant superstructures such as periodic nanoporous films [148], 2D superlattices [149], van der Waals superlattices of transition metal dichalcogenides [150], SiGe nanowires [151] can also be found in the literature.

Early experiments show Si/Ge and GaAs/AlAs superlattices have smaller thermal conductivity compared to their bulk counterparts over a wide range of temperatures [34,152]. But whether coherent phonons exist was under debate until the first unambiguous experimental observation in GaAs/AlAs superlattices of constant period but varying sample thickness [153]. As shown in Fig. 4(d), the observed linear increase of thermal conductivity with sample thickness, indicating a ballistic thermal transport at low temperatures where phonon–phonon anharmonic scattering is weak, confirming the existence of phonon modes having MFPs larger than a period immune to interface scattering. Later, a crossover from coherent to incoherent phonon transport has been reported on high-quality epitaxial oxide superlattices featuring a minimum in thermal conductivity against interface density [142]. The characteristics of coherent phonons have been also reported in a variety of superstructures, including Ruddlesdon–Popper phases [154], silicon nitride periodic porous films [155], Ge/Si core–shell nanowires [156], colloidal nanocrystal superlattices [157].

Anderson localization is another phenomenon that could be resulted by the dominance of coherent phonons. As shown in Fig. 4(e), Anderson localization arises from the interference of multiple-wave scatterings in highly disordered systems, where constructive interference can enhance the probability in certain regions, while destructive interference hinders dissipation pathways. In phonon transport, Anderson localization occurs as certain phonon modes transition from propagating to localized due to destructive interference from multiple elastic scattering events. For example, in superlattices, unlike the ballistic effect, as the total thickness of the superlattices increases, some phonons cease propagation and no longer contribute to heat conduction, leading to a decreasing thermal conductivity with increasing thickness. The idea of phonon localization was proposed by Venkatasubramanian's work [158] where the reduction of cross-plane thermal conductivity in Bi_2Te_3/Sb_2Te_3 superlattices is contributed by the localization of low-frequency phonon with Anderson criterion applied on the cutoff frequency, and later follow-up by other simulations [159,160]. In Fig. 4(f), Anderson localization was experimentally observed in disordered GaAs/AlAs superlattices [161,162]. At cryogenic temperatures, the thermal conductivity peaks at a certain sample length before declining against the increase of sample length, featuring Anderson localization. Recently as machine learning methods become increasingly popular, there are studies [163,164] taking advantage of optimization algorithms to search for aperiodic superlattices maximizing Anderson localization for achieving minimum thermal conductivity. These developments on coherent heat conduction and localization unlock the potential to engineer phonon thermal transport in the wave regime as realized for photons and electrons.

6 Interfacial Thermal Transport

Unlike the nonclassical phenomena within materials that cannot be described by the mathematical form of Fourier's law, interfacial thermal transport [33] is generally treated as an extension. In this context, heat flux results in a finite temperature discontinuity at the interface, and the proportionality between heat flux and the temperature jump is characterized by the thermal boundary conductance (TBC, G), or its reverse, the thermal boundary resistance (TBR, R), in the form of $q = G\Delta T = \Delta T/R$, and it can be resulted by interface scattering, incomplete contact, and near-interface disorder (Fig. 5(a)). The importance of TBR is usually evaluated by Kapitza length $L_K = k/G$. For characteristic length scales comparable or smaller than L_K, the interfaces become a vital factor in hindering the thermal transport. The Kapitza length ranges from tens of nanometers for high quality Pd/Ir interface [165] to tens of micrometers for Bi/diamond interface [166], and can be even higher due to the roughness or contamination [167]. In ballistic regime, it is found that the TBR can even depend on the nearby environment, such as other interfaces that selectively filter phonons [168,169]. Therefore, for modern devices with nanoscale features, the TBR is a critical parameter that needs to be carefully considered and improved.

Analytical formulations of the thermal boundary resistance (TBR) mainly include two models, the acoustic mismatch model (AMM) and the diffuse mismatch model (DMM) [170]. The AMM follows the elastic wave theory, giving the transmission coefficient of phonons across the interface as:

$$\alpha_{12}(\theta, s) = \frac{4 \frac{\rho_2 v_{s,2}}{\rho_1 v_{s,1}} \frac{\cos \theta_{s,2}}{\cos \theta_{s,1}}}{\left(\frac{\rho_2 v_{s,2}}{\rho_1 v_{s,1}} + \frac{\cos \theta_{s,2}}{\cos \theta_{s,1}} \right)^2}$$

where ρ, v are the density and phonon group velocity, respectively. The subscripts 1 and 2 denote the two materials, and s is the phonon branch index. The angle θ is the angle between the phonon wavevector and the interface normal. The AMM is valid for low

temperature cases where long-wavelength acoustic phonons dominate the heat transport. The DMM, on the other hand, assumes that phonons lose memory of their original direction and polarization once they are scattered at the interface. The transmission coefficient in the DMM is given by

$$\alpha_{12} = \frac{\sum_s v_{s,2}^{-2}}{\sum_s v_{s,1}^{-2} + \sum_s v_{s,2}^{-2}},$$

where the summation is over all phonon branches. DMM is valid for higher temperature and rough interfaces where the phonon scattering on the interface is more diffusive and isotropic.

Despite that both AMM and DMM are simplified models, it can be seen from them that the transmission coefficient is higher when the phonon bands of the two materials are more similar, leading to lower TBR, vice versa. For example, the Debye temperature of diamond is approximately 2000 K, which is significantly higher than that of materials employed in the semiconductor industry, resulting in high TBR between diamond and these materials. Contrarily, BAs and BP exhibit lower Debye temperature, suggesting a potentially lower TBR with more matched phonon DoS, and is confirmed by both atomistic modeling and experimental investigations [24].

For numerical calculations of TBR, MD and AGF are widely applied methods. Mingo and Yang [32] employed AGF and solves the transmission coefficient for each phonon mode using the harmonic matrices of the contacts and device. However, the consideration of anharmonicity requires significant effort with substantially growing degrees of freedom [171]. MD simulations for TBR are twofold, i.e., equilibrium MD (EMD) [29] and NEMD [28]. Similar with the determination of thermal conductivity, the Green-Kubo formula can also be extended to the calculations of TBR, while NEMD generally applies two thermal reservoirs to the system under simulation, and extracts the heat flux and temperature jump at the interface. LD, on the other hand, involves substituting plane-wave solutions to represent the incident, reflected, and transmitted waves at an interface [172–174]. The amplitudes of these plane waves are then determined by applying boundary conditions or solving the equations of motion for the atoms located near the interface. However, due to the lack of anharmonicity, LD is restricted to low temperatures. All three methods rely on accurate interatomic forces that can be either empirical or computed by DFT. However, it should be noticed that empirical potentials are usually fitted to reproduce one or some of material properties, thus could lead to unreasonable results for other properties. Strides have been made toward the improvement of interatomic potential. For example, a reactive force field [175] is developed based on quantum mechanical principles, and it can even characterize bond formation and breaking. Recently, considerable work has been done to develop machine learning interatomic potentials [176,177] that are trained by DFT calculations and are able to provide similar accuracy levels with ab initio calculations. Nevertheless, it is important to acknowledge that, in any case, there could be a tradeoff between accuracy and computational cost.

Experimentally, thermal interface and TBR has been well studied for both fundamental interface properties and thermal interface applications [33]. Early steady-state measurements of TBR involves with the heater-sensor method, that is to measure the temperature difference in response to a given heat flow [170,178]. The sensors can be thermocouples, thermistor, or infrared thermometers, and it usually requires the sample to be at a large size scale, resulting in the difficulty to measure micro- and nanoscale sample. An improved technique to perform steady-state measurements at nanoscale is the T-type method [179–181], which uses a hot wire to serve as both the heater and the sensor. Later, the transient 3ω method [182–184] is extensively employed to measure both thermal conductivity and the TBR. The 3ω method uses an AC at frequency ω to produce Joule heating at frequency 2ω, then extract 3ω responses to analyze thermal properties. Comparing with the steady-states measurements, the 3ω method can significantly exclude the error introduced

by radiative heat transfer. However, extra thermal resistance can also be introduced by additional insulating layer that electrically isolates the sample [33]. Based on ultrafast optics, thermal measurements have been greatly advanced by the transient thermoreflectance technique, especially TDTR [34–37] and FDTR [38,185]. FDTR applies a varied frequency difference between the pump and the probe lasers, while TDTR introduces a delay time between the two lasers, and they both extract thermal properties by fitting a corresponding heat conduction model. Due to the high sensitivity and reliability, TDTR has been broadly used to study interfacial thermal transport phenomena, for example, interfaces comprising low-dimensional materials [186,187], anisotropic interfacial phonon transport (Figs. 5(b) and 5(c)) [30], and dynamic tuning of TBR (Figs. 5(d) and 5(e)) [6].

7 Near-Field Radiation

In addition to the phonon-mediated heat transport, radiative heat transfer can also behave different manners at small scales. When two objects are closely spaced, the radiative heat transfer between them can be enhanced by the tunneling of evanescent waves, and the blackbody radiation limit can be surpassed [188]. This phenomenon is known as near-field radiation, and has attracted much attention in recent years, especially in the context of nanoscale heat transfer. Theoretical investigations into near-field radiation are mainly based on Polder and Van Hove's work [189] that is originated from the fluctuational electrodynamics (FE) formulation [190]. For two closely placed parallel plates, the heat flux across the gap d is

$$q = \int_0^\infty \int_0^\infty \left(\frac{\hbar\omega}{e^{\hbar\omega/k_B T}} \right) \tau(\omega, \kappa, d) \frac{\kappa d\kappa}{2\pi} \frac{d\omega}{2\pi}$$

where $\tau = \tau_s + \tau_p$ it the total transmission that incorporates the transverse electric (TE, s) mode and the transverse magnetic (TM, p) mode. κ is the in-plane wave number, the integral with respect to κ thus includes both propagating waves ($\kappa \leq \omega/c$) and evanescent waves ($\kappa > \omega/c$). The transmission coefficient for evanescent waves decays exponentially, the heat flux thus approaches black-body limit when the gap is sufficiently large. However, for the near-field situations, the contribution due to evanescent waves can be significant. The critical size scale can be measured by λ_{Th} that is the result of Wien displacement law. In addition to parallel plates, other geometries such as point-to-surface [191] and sphere-to-substrate [192] are also studied.

The first experiments were carried by Tien and coworkers [193,194] at cryogenic temperatures between two copper plates, they measured heat transfer rates as a function of gap size ranging from 2 mm to 10 μm, and found that the heat flow monotonically increases with decreasing gap size. At room temperature, Hargreaves [195] observed the enhanced heat transfer between two metal plates by adjusting the gap size at micrometer scale. However, due to the large surfaces, Hargreaves could not reach distances smaller than 1.5 μm. Xu et al. [196] applied the piezotube of a scanning tunneling microscope head to control the gap size, enabling the measurements between 1.5 μm down to mechanical contact, and it is found that heat transfer can saturate when the gap size is as small as tens of nanometers. Later, Kittel et al. [197] used a gold tip to measure the heat transfer between the tip and a surface. The measurements for the gold sample and the GaN sample suggest several orders of magnitude of enhanced near-field radiation at nanoscale. However, below 10 nm, the results differ markedly from the prediction of FE, revealing that the macroscopic description of the dielectric properties fails at nanoscale. At temperatures higher
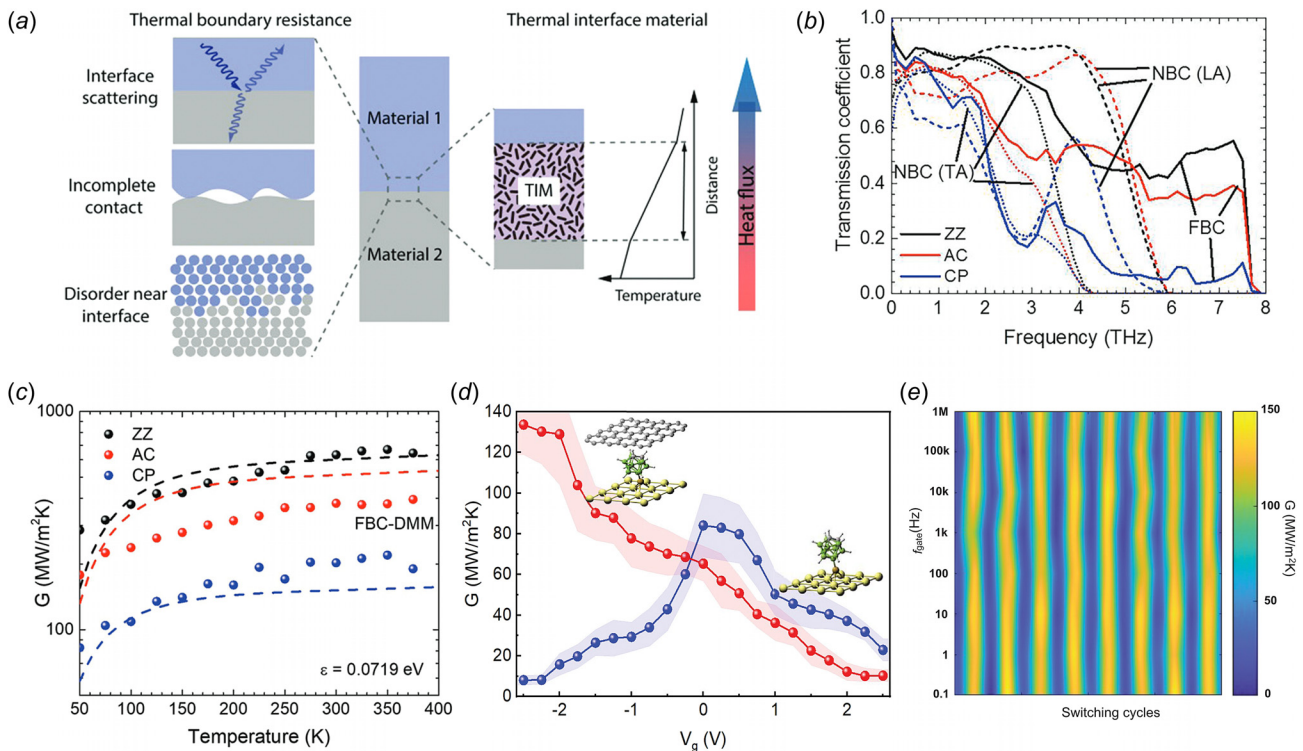

Fig. 5 Interface thermal transport and dynamic tuning. (a) Schematic shows the multiscale contributions to interfacial thermal transport and a lumped TBR, including the atomistic interface scattering to incomplete microscale contacts and disorders near the interface. Adapted from *J. Mater. Chem. C*, 8, 10568, 2020. (b, c) Anisotropic TBR, adapted from *Advanced Materials* 31, 1901021, 2019. (b) Atomistic modeling considering phonon mode dependent interface transmission; (c) experimental measurements and MD simulation results of temperature dependent TBR, along varied crystal orientation of black phosphorus. (d, e) Dynamic thermal tuning and electrically gated thermal switch, adapted from *Science* 382, 585, 2023. (d) The measured thermal conductance as a function of gate voltage. Inset, High-resolution cross-sectional TEM image of the device structure showing the atomically resolved interface. (e) High–switching speed measurements, plotting thermal switching cycles versus scanning frequency response up to 1 MHz, measured at every decade.

than room temperature, Hu et al. [198] reported that the blackbody limit is exceeded by near-field radiation for two glassy plates.

The experimental studies of near-field radiation are challenged by the relatively small radiative heat transfer rate [199] and the difficulty to control and measure the gap sizes [200–202]. Fortunately, rapidly developing computational studies opened the possibilities of engineering the near-field radiation. For simple curved surfaces, radiative thermal conductance can be estimated by using the Derjaguin approximation [203,204], i.e., to approximate the curved surfaces by differential flat areas. For arbitrary geometries, most widely used approaches include the scattering matrix approach [205–207], the fluctuating surface current formulation [208–210], and the finite difference time domain approach [211,212]. Computational investigations with these methods have revealed the possibilities to use near-field radiation to realize or improve diverse applications, such as thermophotovoltaic generators [213], heat flow modulation [214,215], thermal rectification [216,217], thermal transistors [218].

8 Surface Phonon Polariton

Surface phonon polaritons (SPhPs) are hybrid quasi-particles resulting from the coupling between electromagnetic (EM) waves and optical phonons at the surface of polar dielectric materials. In polar materials, EM waves can couple with atomic vibrations through dipole-dipole interactions. When the frequency of EM waves matches that of the optical phonons, the EM waves resonate with the lattice vibrations, leading to the formation of phonon polaritons. The SPhPs are confined to the interface between metals and dielectric polar materials, because the amplitude of EM waves decays exponentially within the bulk dielectric material due to the inherent material properties, including optical absorption and the dielectric function of the material. Metals plays a crucial role in the formation of SPhPs since they can provide a high density of free electrons that can interact with EM wave. SPhPs have garnered significant attention due to their potential applications in nanophotonics, thermal management, and infrared optics. Especially, the SPhPs are being explored as potential novel energy carriers to enhance heat conduction.

The SPhPs are known to have long propagation lengths, especially in thin films [219,220]. The properties of SPhP, including their dispersion relation and propagation length, were determined using Maxwell equations by Yang et al. [221] In 2005, Chen et al. [222] analyzed the heat conduction capabilities of SPhP and found that SPhPs along SiO_2 thin films could enhance the thermal conductivity by several folds due to their exceptionally long propagation lengths compared to phonons. Many subsequent theoretical investigations into the thermal transport of SPhPs have been conducted by Volz et al., such as the SPhPs in asymmetric surrounding media [223], quantum conductance of SPhP [224], and SPhP in assembly of spheroidal nanoparticles [225]. Yun et al. [226] studied the size effects on the thermal transport of SPhPs by solving the spectral-dependent BTE.

Several experiments have been conducted to explore the thermal transport of SPhPs. Chen et al. [227] measured the propagation length of SPhPs, showing it can reach up to 10.8 μm on silicon dioxide thin films. The thermal conductivity of silica thin films and SiN nanomembranes was observed to increase by up to twofold due to the presence of SPhPs [228,229]. In SiN nanomembranes, the propagation length of SPhPs was demonstrated to reach hundreds of micrometers [230]. In SiO_2 nanoribbons, non-Fourier behavior resulted by SPhPs in over 50–100 μm distance at room and high temperature is captured [231]. In 2023, the thermal conductance of 3 C-SiC nanowires coated with gold was measured to be more than two orders of magnitude higher than the Landauer limit, with the remarkable enhancement attributed to nonequilibrium SPhPs [232].

Surface phonon polaritons represent a fascinating intersection of optics and phononics, offering unique opportunities as novel energy carriers to enhance heat conduction at the nanoscale. Ongoing investigations and developments are expected to have a profound impact on thermal management.

9 Conclusion and Outlook

Heat transfer beyond classical Fourier's law has been extensively studied over the past decades to address the growing demands of thermal management and the pressing need to understand transport physics at the nanoscale. This review briefly summarizes key phenomena that deviate from the classical regime, including those arising from the particle-like behavior of phonons, such as ballistic transport, phonon hydrodynamics, and interfacial and surface thermal transport. It also covers phenomena associated with the wave-like behavior of phonons, such as coherent phonon transport and phonon localization. Additionally, advances in near-field radiation are discussed.

The dual nature of phonons, exhibiting both particle-like and wave-like characteristics, is fundamental to their quantum behavior, and the interplay between these behaviors is crucial for understanding heat transfer. Beyond the phonon BTE, recent efforts are developing new approaches such as unified formulation of the Wigner Transport Equation, which shows promise in characterizing heat transport that encompasses both particle-like and wave-like properties in ordered and disordered materials. However, the complexities involved in solving the transient Wigner Transport Equation for real-world materials of finite size remain a significant challenge, highlighting an opportunity for further research and innovation in this field. Alternatively, approaches that combine rigorous calculation such as ab initio theory with high-throughput processing such as machine learning modeling may provide benefit for certain areas [233].

In addition to established phenomena, emerging areas of research such as chiral phonons and topological phonons offer exciting prospects for advancing phonon engineering. Chiral phonons [234–236], which possess angular momentum and exhibit unique coupling with electronic and magnetic degrees-of-freedom, could enable novel mechanisms for controlling thermal conductivity in materials with broken inversion symmetry. Topological phonons [237–239], characterized by their robust edge states protected by the material's topological properties, present another frontier for manipulating heat transport with unprecedented precision. These phenomena not only expand our understanding of phononic behavior but also open up new possibilities for designing materials with tailored thermal properties, potentially leading to groundbreaking applications in electronics thermal management and quantum technologies.

Data Availability Statement

The authors attest that all data for this study are included in the paper.

References

[1] Fourier, J. B. J., 1822, *Théorie Analytique de La Chaleur*, Chez Firmin Didot, Père et Fils, Paris.
[2] Bergman, T. L., and Incropera, F. P., 2011, *Fundamentals of Heat and Mass Transfer*, Wiley, Hoboken, NJ.
[3] Chen, G., 2005, *Nanoscale Energy Transport and Conversion: A Parallel Treatment of Electrons, Molecules, Phonons, and Photons*, Oxford University Press, New York.
[4] Kang, J. S., Li, M., Wu, H., Nguyen, H., and Hu, Y., 2018, "Experimental Observation of High Thermal Conductivity in Boron Arsenide," Science, **361** (6402), pp. 575–578.

[5] Li, S., Qin, Z., Wu, H., Li, M., Kunz, M., Alatas, A., Kavner, A., and Hu, Y., 2022, "Anomalous Thermal Transport Under High Pressure in Boron Arsenide," Nature, **612**(7940), pp. 459–464.

[6] Li, M., Wu, H., Avery, E. M., Qin, Z., Goronzy, D. P., Nguyen, H. D., Liu, T., Weiss, P. S., and Hu, Y., 2023, "Electrically Gated Molecular Thermal Switch," Science, **382**(6670), pp. 585–589.

[7] Peierls, R., 1929, "Zur Kinetischen Theorie Der Wärmeleitung in Kristallen," Ann. Phys., **395**(8), pp. 1055–1101.

[8] Srivastava, G. P., 2022, *The Physics of Phonons*, CRC Press, Boca Raton.

[9] Simoncelli, M., Marzari, N., and Mauri, F., 2019, "Unified Theory of Thermal Transport in Crystals and Glasses," Nat. Phys., **15**(8), pp. 809–813.

[10] Simoncelli, M., Marzari, N., and Mauri, F., 2022, "Wigner Formulation of Thermal Transport in Solids," Phys. Rev. X, **12**(4), p. 41011.

[11] Broido, D. A., Malorny, M., Birner, G., Mingo, N., and Stewart, D. A., 2007, "Intrinsic Lattice Thermal Conductivity of Semiconductors From First Principles," Appl. Phys. Lett., **91**(23), p. 231922.

[12] Garg, J., Bonini, N., Kozinsky, B., and Marzari, N., 2011, "Role of Disorder and Anharmonicity in the Thermal Conductivity of Silicon-Germanium Alloys: A First-Principles Study," Phys. Rev. Lett., **106**(4), p. 045901.

[13] Esfarjani, K., Chen, G., and Stokes, H. T., 2011, "Heat Transport in Silicon From First-Principles Calculations," Phys. Rev. B—Condens. Matter Mater. Phys., **84**(8), p. 85204.

[14] Lindsay, L., Broido, D. A., and Reinecke, T. L., 2013, "First-Principles Determination of Ultrahigh Thermal Conductivity of Boron Arsenide: A Competitor for Diamond?," Phys. Rev. Lett., **111**(2), p. 025901.

[15] Feng, T., Lindsay, L., and Ruan, X., 2017, "Four-Phonon Scattering Significantly Reduces Intrinsic Thermal Conductivity of Solids," Phys. Rev. B, **96**(16), p. 161201.

[16] Fan, H., Wu, H., Lindsay, L., and Hu, Y., 2019, "Ab Initio Investigation of Single-Layer High Thermal Conductivity Boron Compounds," Phys. Rev. B, **100**(8), p. 085420.

[17] Kang, J. S., Wu, H., Li, M., and Hu, Y., 2019, "Intrinsic Low Thermal Conductivity and Phonon Renormalization Due to Strong Anharmonicity of Single-Crystal Tin Selenide," Nano Lett., **19**(8), pp. 4941–4948.

[18] Wu, H., Fan, H., and Hu, Y., 2021, "Ab Initio Determination of Ultrahigh Thermal Conductivity in Ternary Compounds," Phys. Rev. B, **103**(4), p. L041203.

[19] Wu, H., Qin, Z., Li, S., Lindsay, L., and Hu, Y., 2023, "Nonperturbative Determination of Isotope-Induced Anomalous Vibrational Physics," Phys. Rev. B, **108**(14), p. L140302.

[20] Peterson, R. B., 1994, "Direct Simulation of Phonon-Mediated Heat Transfer in a Debye Crystal," ASME J. Heat Mass Transfer-Trans. ASME, **116**(4), pp. 815–822.

[21] Mazumder, S., and Majumdar, A., 2001, "Monte Carlo Study of Phonon Transport in Solid Thin Films Including Dispersion and Polarization," ASME J. Heat Mass Transfer-Trans. ASME, **123**(4), pp. 749–759.

[22] Péraud, J.-P. M., and Hadjiconstantinou, N. G., 2011, "Efficient Simulation of Multidimensional Phonon Transport Using Energy-Based Variance-Reduced Monte Carlo Formulations," Phys. Rev. B, **84**(20), p. 205331.

[23] Hu, Y., Zeng, L., Minnich, A. J., Dresselhaus, M. S., and Chen, G., 2015, "Spectral Mapping of Thermal Conductivity Through Nanoscale Ballistic Transport," Nat. Nanotechnol., **10**(8), pp. 701–706.

[24] Kang, J. S., Li, M., Wu, H., Nguyen, H., Aoki, T., and Hu, Y., 2021, "Integration of Boron Arsenide Cooling Substrates Into Gallium Nitride Devices," Nat. Electron., **4**(6), pp. 416–423.

[25] Landon, C. D., and Hadjiconstantinou, N. G., 2014, "Deviational Simulation of Phonon Transport in Graphene Ribbons With Ab Initio Scattering," J. Appl. Phys., **116**, p. 163502.

[26] Wu, H., and Hu, Y., 2024, "Ab Initio Investigations on Hydrodynamic Phonon Transport: From Diffusion to Convection," Int. J. Heat Mass Transfer, **220**, p. 124988.

[27] Henry, A. S., and Chen, G., 2008, "Spectral Phonon Transport Properties of Silicon Based on Molecular Dynamics Simulations and Lattice Dynamics," J. Comput. Theor. Nanosci., **5**(2), pp. 141–152.

[28] Landry, E. S., and McGaughey, A. J. H., 2009, "Thermal Boundary Resistance Predictions From Molecular Dynamics Simulations and Theoretical Calculations," Phys. Rev. B, **80**(16), p. 165304.

[29] Rajabpour, A., and Volz, S., 2010, "Thermal Boundary Resistance From Mode Energy Relaxation Times: Case Study of Argon-Like Crystals by Molecular Dynamics," J. Appl. Phys., **108**(9), p. 094324.

[30] Li, M., Kang, J. S., Nguyen, H. D., Wu, H., Aoki, T., and Hu, Y., 2019, "Anisotropic Thermal Boundary Resistance Across 2D Black Phosphorus: Experiment and Atomistic Modeling of Interfacial Energy Transport," Adv. Mater., **31**(33), p. 1901021.

[31] Qin, Z., Dai, L., Li, M., Li, S., Wu, H., White, K. E., Gani, G., Weiss, P. S., and Hu, Y., 2024, "Moiré Pattern Controlled Phonon Polarizer Based on Twisted Graphene," Adv. Mater., **36**(24), p. 2312176.

[32] Mingo, N., and Yang, L., 2003, "Phonon Transport in Nanowires Coated With an Amorphous Material: An Atomistic Green's Function Approach," Phys. Rev. B, **68**(24), p. 245406.

[33] Cui, Y., Li, M., and Hu, Y., 2020, "Emerging Interface Materials for Electronics Thermal Management: Experiments, Modeling, and New Opportunities," J. Mater. Chem. C Mater., **8**(31), pp. 10568–10586.

[34] Capinski, W. S., and Maris, H. J., 1996, "Thermal Conductivity of GaAs/AlAs Superlattices," Phys. B Condens. Matter, **219–220**, pp. 699–701.

[35] Cahill, D. G., 2004, "Analysis of Heat Flow in Layered Structures for Time-Domain Thermoreflectance," Rev. Sci. Instrum., **75**(12), pp. 5119–5122.

[36] Schmidt, A. J., Chen, X., and Chen, G., 2008, "Pulse Accumulation, Radial Heat Conduction, and Anisotropic Thermal Conductivity in Pump-Probe Transient Thermoreflectance," Rev. Sci. Instrum., **79**(11), p. 114902.

[37] Li, M., Kang, J. S., and Hu, Y., 2018, "Anisotropic Thermal Conductivity Measurement Using a New Asymmetric-Beam Time-Domain Thermoreflectance (AB-TDTR) Method," Rev. Sci. Instrum., **89**(8), p. 084901.

[38] Schmidt, A. J., Cheaito, R., and Chiesa, M., 2009, "A Frequency-Domain Thermoreflectance Method for the Characterization of Thermal Properties," Rev. Sci. Instrum., **80**(9), p. 094901.

[39] Rogers, J. A., Maznev, A. A., Banet, M. J., and Nelson, K. A., 2000, "Optical Generation and Characterization of Acoustic Waves in Thin Films: Fundamentals and Applications," Annu. Rev. Mater. Sci., **30**(1), pp. 117–157.

[40] Cui, L., Hur, S., Akbar, Z. A., Klöckner, J. C., Jeong, W., Pauly, F., Jang, S.-Y., Reddy, P., and Meyhofer, E., 2019, "Thermal Conductance of Single-Molecule Junctions," Nature, **572**(7771), pp. 628–633.

[41] Bhatnagar, P. L., Gross, E. P., and Krook, M., 1954, "A Model for Collision Processes in Gases. I. Small Amplitude Processes in Charged and Neutral One-Component Systems," Phys. Rev., **94**(3), pp. 511–525.

[42] Casimir, H. B. G., 1938, "Note on the Conduction of Heat in Crystals," Physica, **5**(6), pp. 495–500.

[43] Jeong, C., Datta, S., and Lundstrom, M., 2012, "Thermal Conductivity of Bulk and Thin-Film Silicon: A Landauer Approach," J. Appl. Phys., **111**(9), p. 093708.

[44] Lindsay, L., 2016, "First Principles Peierls-Boltzmann Phonon Thermal Transport: A Topical Review," Nanoscale Microscale Thermophys. Eng., **20**(2), pp. 67–84.

[45] Mingo, N., and Broido, D. A., 2004, "Lattice Thermal Conductivity Crossovers in Semiconductor Nanowires," Phys. Rev. Lett., **93**(24), p. 246106.

[46] Ward, A., Broido, D. A., Stewart, D. A., and Deinzer, G., 2009, "Ab Initio Theory of the Lattice Thermal Conductivity in Diamond," Phys. Rev. B—Condens. Matter Mater. Phys., **80**(12), p. 125203.

[47] Lindsay, L., Broido, D. A., and Reinecke, T. L., 2012, "Thermal Conductivity and Large Isotope Effect in GaN From First Principles," Phys. Rev. Lett., **109**(9), p. 095901.

[48] Ke, M., Nguyen, H., and Hu, Y., 2020, "Complementary doping of van der Waals materials through controlled intercalation for monolithically integrated electronics," Nano Res., **13**, pp. 1369–1375.

[49] Klitsner, T., VanCleve, J. E., Fischer, H. E., and Pohl, R. O., 1988, "Phonon Radiative Heat Transfer and Surface Scattering," Phys. Rev. B, **38**(11), pp. 7576–7594.

[50] Joshi, A. A., and Majumdar, A., 1993, "Transient Ballistic and Diffusive Phonon Heat Transport in Thin Films," J. Appl. Phys., **74**(1), pp. 31–39.

[51] Majumdar, A., 1993, "Microscale Heat Conduction in Dielectric Thin Films," ASME J. Heat Mass Transfer-Trans. ASME, **115**(1), pp. 7–16.

[52] Chen, G., 1996, "Nonlocal and Nonequilibrium Heat Conduction in the Vicinity of Nanoparticles," ASME J. Heat Mass Transfer-Trans. ASME, **118**(3), pp. 539–545.

[53] Maassen, J., and Lundstrom, M., 2015, "Steady-State Heat Transport: Ballistic-to-Diffusive With Fourier's Law," J. Appl. Phys., **117**(3), p. 035104.

[54] Maassen, J., and Lundstrom, M., 2015, "A Simple Boltzmann Transport Equation for Ballistic to Diffusive Transient Heat Transport," J. Appl. Phys., **117**(13), p. 135102.

[55] Chen, G., 2001, "Ballistic-Diffusive Heat-Conduction Equations," Phys. Rev. Lett., **86**(11), pp. 2297–2300.

[56] Chen, G., 2002, "Ballistic-Diffusive Equations for Transient Heat Conduction From Nano to Macroscales," ASME J. Heat Mass Transfer-Trans. ASME, **124**(2), pp. 320–328.

[57] Cattaneo, C., 1948, "Sulla Conduzione Del Calore," Atti Sem. Mat. Fis. Univ. Modena, **3**, pp. 83–101.

[58] Vernotte, P., 1958, "Les Paradoxes de La Theorie Continue de L'equation de La Chaleur," C. R., **246**, pp. 3154–3155.

[59] Alvarez, F. X., and Jou, D., 2007, "Memory and Nonlocal Effects in Heat Transport: From Diffusive to Ballistic Regimes," Appl. Phys. Lett., **90**(8), p. 083109.

[60] Kresse, G., and Furthmüller, J., 1996, "Efficient Iterative Schemes for ab Initio Total-Energy Calculations Using a Plane-Wave Basis Set," Phys. Rev. B, **54**(16), pp. 11169–11186.

[61] Kresse, G., and Joubert, D., 1999, "From Ultrasoft Pseudopotentials to the Projector Augmented-Wave Method," Phys. Rev. B, **59**(3), pp. 1758–1775.

[62] Giannozzi, P., Baroni, S., Bonini, N., Calandra, M., Car, R., Cavazzoni, C., Ceresoli, D., et al., 2009, "QUANTUM ESPRESSO: A Modular and Open-Source Software Project for Quantum Simulations of Materials," J. Phys.: Condens. Matter, **21**, p. 395502.

[63] Giannozzi, P., Andreussi, O., Brumme, T., Bunau, O., Buongiorno Nardelli, M., Calandra, M., Car, R., et al., 2017, "Advanced Capabilities for Materials Modelling With QUANTUM ESPRESSO," J. Phys.: Condens. Matter, **29**(46), p. 465901.

[64] Giannozzi, P., Baseggio, O., Bonfà, P., Brunato, D., Car, R., Carnimeo, I., Cavazzoni, C., et al., 2020, "Quantum ESPRESSO Toward the Exascale," J. Chem. Phys., **152**(15), p. 154105.

[65] Kühne, T. D., Iannuzzi, M., Del Ben, M., Rybkin, V. V., Seewald, P., Stein, F., Laino, T., et al., 2020, "CP2K: An Electronic Structure and Molecular Dynamics Software package-Quickstep: Efficient and Accurate Electronic Structure Calculations," J. Chem. Phys., **152**(19), p. 194103.

[66] Gonze, X., Amadon, B., Antonius, G., Arnardi, F., Baguet, L., Beuken, J.-M., Bieder, J., et al., 2020, "The ABINIT Project: Impact, Environment and Recent Developments," Comput. Phys. Commun., **248**, p. 107042.

[67] Boker, S., Neale, M., Maes, H., Wilde, M., Spiegel, M., Brick, T., Spies, J., et al., 2011, "OpenMx: An Open Source Extended Structural Equation Modeling Framework," Psychometrika, **76**(2), pp. 306–317.

[68] Tadano, T., Gohda, Y., and Tsuneyuki, S., 2014, "Anharmonic Force Constants Extracted From First-Principles Molecular Dynamics: Applications to Heat Transfer Simulations," J. Phys.: Condens. Matter, **26**(22), p. 225402.

[69] Togo, A., 2023, "First-Principles Phonon Calculations With Phonopy and Phono3py," J. Phys. Soc. Jpn., **92**(1), p. 12001.

[70] Togo, A., Chaput, L., Tadano, T., and Tanaka, I., 2023, "Implementation Strategies in Phonopy and phono3py," J. Phys. Condens. Matter, **35**(35), p. 353001.

[71] Li, W., Carrete, J., Katcho, N. A., and Mingo, N., 2014, "ShengBTE: A Solver of the Boltzmann Transport Equation for Phonons," Comp. Phys. Commun., **185**(6), pp. 1747–1758.

[72] Han, Z., Yang, X., Li, W., Feng, T., and Ruan, X., 2022, "FourPhonon: An Extension Module to ShengBTE for Computing Four-Phonon Scattering Rates and Thermal Conductivity," Comput. Phys. Commun., **270**, p. 108179.

[73] Bao, H., Chen, J., Gu, X., and Cao, B., 2018, "A Review of Simulation Methods in Micro/Nanoscale Heat Conduction," ES Energy Environ., **1**(84), pp. 16–55.

[74] Péraud, J.-P. M., and Hadjiconstantinou, N. G., 2012, "An Alternative Approach to Efficient Simulation of Micro/Nanoscale Phonon Transport," Appl. Phys. Lett., **101**, p. 153114.

[75] Hua, Y.-C., and Cao, B.-Y., 2016, "Ballistic-Diffusive Heat Conduction in Multiply-Constrained Nanostructures," Int. J. Therm. Sci., **101**, pp. 126–132.

[76] Kang, J. S., Wu, H., and Hu, Y., 2017, "Thermal Properties and Phonon Spectral Characterization of Synthetic Boron Phosphide for High Thermal Conductivity Applications," Nano Lett., **17**(12), pp. 7507–7514.

[77] Murthy, J. Y., and Mathur, S. R., 2002, "Computation of Sub-Micron Thermal Transport Using an Unstructured Finite Volume Method," ASME J. Heat Mass Transfer-Trans. ASME, **124**(6), pp. 1176–1181.

[78] Romano, G., 2021, "Openbte: A Solver for ab-Initio Phonon Transport in Multidimensional Structures," arXiv:2106.02764.

[79] Narumanchi, S. V. J., Murthy, J. Y., and Amon, C. H., 2003, "Simulation of Unsteady Small Heat Source Effects in Sub-Micron Heat Conduction," ASME J. Heat Mass Transfer-Trans. ASME, **125**(5), pp. 896–903.

[80] Guo, Y., and Wang, M., 2017, "Heat Transport in Two-Dimensional Materials by Directly Solving the Phonon Boltzmann Equation Under Callaway's Dual Relaxation Model," Phys. Rev. B, **96**(13), p. 134312.

[81] Guo, Y., Zhang, Z., Nomura, M., Volz, S., and Wang, M., 2021, "Phonon Vortex Dynamics in Graphene Ribbon by Solving Boltzmann Transport Equation With ab Initio Scattering Rates," Int. J. Heat Mass Transfer, **169**, p. 120981.

[82] Luo, X.-P., Guo, Y.-Y., Wang, M.-R., and Yi, H.-L., 2019, "Direct Simulation of Second Sound in Graphene by Solving the Phonon Boltzmann Equation Via a Multiscale Scheme," Phys. Rev. B, **100**(15), p. 155401.

[83] Feng, T., Yao, W., Wang, Z., Shi, J., Li, C., Cao, B., and Ruan, X., 2017, "Spectral Analysis of Nonequilibrium Molecular Dynamics: Spectral Phonon Temperature and Local Nonequilibrium in Thin Films and Across Interfaces," Phys. Rev. B, **95**(19), p. 195202.

[84] Hu, Y., Feng, T., Gu, X., Fan, Z., Wang, X., Lundstrom, M., Shrestha, S. S., and Bao, H., 2020, "Unification of Nonequilibrium Molecular Dynamics and the Mode-Resolved Phonon Boltzmann Equation for Thermal Transport Simulations," Phys. Rev. B, **101**(15), p. 155308.

[85] Xu, J., Hu, Y., Ruan, X., Wang, X., Feng, T., and Bao, H., 2021, "Nonequilibrium Phonon Transport Induced by Finite Sizes: Effect of Phonon-Phonon Coupling," Phys. Rev. B, **104**(10), p. 104310.

[86] Feng, T., Zhong, Y., Shi, J., and Ruan, X., 2019, "Unexpected High Inelastic Phonon Transport Across Solid-Solid Interface: Modal Nonequilibrium Molecular Dynamics Simulations and Landauer Analysis," Phys. Rev. B, **99**(4), p. 045301.

[87] Asheghi, M., Leung, Y. K., Wong, S. S., and Goodson, K. E., 1997, "Phonon-Boundary Scattering in Thin Silicon Layers," Appl. Phys. Lett., **71**(13), pp. 1798–1800.

[88] Ju, Y. S., and Goodson, K. E., 1999, "Phonon Scattering in Silicon Films With Thickness of Order 100 nm," Appl. Phys. Lett., **74**(20), pp. 3005–3007.

[89] Johnson, J. A., Maznev, A. A., Cuffe, J., Eliason, J. K., Minnich, A. J., Kehoe, T., Torres, C. M. S., Chen, G., and Nelson, K. A., 2013, "Direct Measurement of Room-Temperature Nondiffusive Thermal Transport Over Micron Distances in a Silicon Membrane," Phys. Rev. Lett., **110**(2), p. 25901.

[90] Minnich, A. J., 2012, "Determining Phonon Mean Free Paths From Observations of Quasiballistic Thermal Transport," Phys. Rev. Lett., **109**(20), p. 205901.

[91] Dames, C., and Chen, G., 2006, "Thermal Conductivity of Nanostructured Thermoelectric Materials," Thermoelectrics Handbook, D. M. Rowe, ed., CRC Press, Boca Raton, FL.

[92] Yang, F., and Dames, C., 2013, "Mean Free Path Spectra as a Tool to Understand Thermal Conductivity in Bulk and Nanostructures," Phys. Rev. B, **87**(3), p. 035437.

[93] Zeng, L., Collins, K. C., Hu, Y., Luckyanova, M. N., Maznev, A. A., Huberman, S., Chiloyan, V., et al., 2015, "Measuring Phonon Mean Free Path Distributions by Probing Quasiballistic Phonon Transport in Grating Nanostructures," Sci. Rep., **5**(1), p. 17131.

[94] Peshkov, V., 1944, "Second Sound in Helium II," J. Phys. USSR, **8**, p. 381.

[95] Ackerman, C. C., Bertman, B., Fairbank, H. A., and Guyer, R. A., 1966, "Second Sound in Solid Helium," Phys. Rev. Lett., **16**(18), pp. 789–791.

[96] McNelly, T. F., Rogers, S. J., Channin, D. J., Rollefson, R. J., Goubau, W. M., Schmidt, G. E., Krumhansl, J. A., and Pohl, R. O., 1970, "Heat Pulses in NaF: Onset of Second Sound," Phys. Rev. Lett., **24**(3), pp. 100–102.

[97] Pohl, D. W., and Irniger, V., 1976, "Observation of second sound in NaF by Means of Light Scattering," Phys. Rev. Lett., **36**(9), pp. 480–483.

[98] Narayanamurti, V., and Dynes, R. C., 1972, "Observation of Second Sound in Bismuth," Phys. Rev. Lett., **28**(22), pp. 1461–1465.

[99] Huberman, S., Duncan, R. A., Chen, K., Song, B., Chiloyan, V., Ding, Z., Maznev, A. A., Chen, G., and Nelson, K. A., 2019, "Observation of Second Sound in Graphite at Temperatures Above 100 K," Science, **364**(6438), pp. 375–379.

[100] Ward, J. C., and Wilks, J., III, 1952, "Second Sound and the Thermo-Mechanical Effect at Very Low Temperatures," London, Edinburgh, Dublin Philos. Mag. J. Sci., **43**(336), pp. 48–50.

[101] Prohofsky, E. W., and Krumhansl, J. A., 1964, "Second-Sound Propagation in Dielectric Solids," Phys. Rev., **133**(5A), pp. A1403–A1410.

[102] Hardy, R. J., 1970, "Phonon Boltzmann Equation and Second Sound in Solids," Phys. Rev. B, **2**(4), pp. 1193–1207.

[103] Guo, Y., and Wang, M., 2015, "Phonon Hydrodynamics and Its Applications in Nanoscale Heat Transport," Phys. Rep., **595**, pp. 1–44.

[104] Callaway, J., 1959, "Model for Lattice Thermal Conductivity at Low Temperatures," Phys. Rev., **113**(4), pp. 1046–1051.

[105] Peierls, R. E., 1955, Quantum Theory of Solids, Oxford University Press, London.

[106] Maznev, A. A., and Wright, O. B., 2014, "Demystifying Umklapp vs Normal Scattering in Lattice Thermal Conductivity," Am. J. Phys., **82**(11), pp. 1062–1066.

[107] Allen, P. B., 2013, "Improved Callaway Model for Lattice Thermal Conductivity," Phys. Rev. B, **88**(14), p. 144302.

[108] Ma, J., Li, W., and Luo, X., 2014, "Examining the Callaway Model for Lattice Thermal Conductivity," Phys. Rev. B, **90**(3), p. 035203.

[109] Fugallo, G., Cepellotti, A., Paulatto, L., Lazzeri, M., Marzari, N., and Mauri, F., 2014, "Thermal Conductivity of Graphene and Graphite: Collective Excitations and Mean Free Paths," Nano Lett., **14**(11), pp. 6109–6114.

[110] Li, X., and Lee, S., 2018, "Role of Hydrodynamic Viscosity on Phonon Transport in Suspended Graphene," Phys. Rev. B, **97**(9), p. 094309.

[111] Simoncelli, M., Marzari, N., and Cepellotti, A., 2020, "Generalization of Fourier's Law Into Viscous Heat Equations," Phys. Rev. X, **10**(1), p. 011019.

[112] Lee, S., Broido, D., Esfarjani, K., and Chen, G., 2015, "Hydrodynamic Phonon Transport in Suspended Graphene," Nat. Commun., **6**(1), p. 6290.

[113] Cepellotti, A., Fugallo, G., Paulatto, L., Lazzeri, M., Mauri, F., and Marzari, N., 2015, "Phonon Hydrodynamics in Two-Dimensional Materials," Nat. Commun., **6**(1), p. 6400.

[114] Ding, Z., Chen, K., Song, B., Shin, J., Maznev, A. A., Nelson, K. A., and Chen, G., 2022, "Observation of Second Sound in Graphite Over 200 K," Nat. Commun., **13**(1), p. 285.

[115] Machida, Y., Matsumoto, N., Isono, T., and Behnia, K., 2020, "Phonon Hydrodynamics and Ultrahigh–Room-Temperature Thermal Conductivity in Thin Graphite," Science, **367**(6475), pp. 309–312.

[116] Allen, P. B., and Feldman, J. L., 1993, "Thermal Conductivity of Disordered Harmonic Solids," Phys. Rev. B, **48**(17), pp. 12581–12588.

[117] Green, M. S., 1952, "Markoff Random Processes and the Statistical Mechanics of Time-Dependent Phenomena," J. Chem. Phys., **20**(8), pp. 1281–1295.

[118] Kubo, R., 1957, "Statistical-Mechanical Theory of Irreversible Processes. I. General Theory and Simple Applications to Magnetic and Conduction Problems," J. Phys. Soc. Jpn., **12**(6), pp. 570–586.

[119] Feldman, J. L., Allen, P. B., and Bickham, S. R., 1999, "Numerical Study of Low-Frequency Vibrations in Amorphous Silicon," Phys. Rev. B, **59**(5), pp. 3551–3559.

[120] Allen, P. B., Feldman, J. L., Fabian, J., and Wooten, F., 1999, "Diffusons, Locons and Propagons: Character of Atomic Vibrations in Amorphous Si," Philos. Mag. B, **79**(11–12), pp. 1715–1731.

[121] Larkin, J. M., and McGaughey, A. J. H., 2014, "Thermal Conductivity Accumulation in Amorphous Silica and Amorphous Silicon," Phys. Rev. B, **89**(14), p. 144303.

[122] Zhou, Y., 2021, "Assessing the Quantum Effect in Classical Thermal Conductivity of Amorphous Silicon," J. Appl. Phys., **129**(23), p. 235104.

[123] Moon, J., 2021, "Examining Normal Modes as Fundamental Heat Carriers in Amorphous Solids: The Case of Amorphous Silicon," J. Appl. Phys., **130**(5), p. 055101.

[124] Cai, Z., Lin, S., Ahmadian-Yazdi, M.-R., and Zhao, C., 2024, "Diffuson-Dominated and Ultra Defect-Tolerant Two-Channel Thermal Transport in Hybrid Halide Perovskites," Adv. Funct. Mater., **34**, p. 2307648.

[125] Shenogin, S., Bodapati, A., Keblinski, P., and McGaughey, A. J. H., 2009, "Predicting the Thermal Conductivity of Inorganic and Polymeric Glasses: The Role of Anharmonicity," J. Appl. Phys., **105**, p. 034906.

[126] He, Y., Donadio, D., and Galli, G., 2011, "Heat Transport in Amorphous Silicon: Interplay Between Morphology and Disorder," Appl. Phys. Lett., **98**, p. 144101.

[127] Liu, X., Feldman, J. L., Cahill, D. G., Crandall, R. S., Bernstein, N., Photiadis, D. M., Mehl, M. J., and Papaconstantopoulos, D. A., 2009, "High Thermal Conductivity of a Hydrogenated Amorphous Silicon Film," Phys. Rev. Lett., **102**(3), p. 035901.

[128] Regner, K. T., Sellan, D. P., Su, Z., Amon, C. H., McGaughey, A. J. H., and Malen, J. A.,, 2013, "Broadband Phonon Mean Free Path Contributions to Thermal Conductivity Measured Using Frequency Domain Thermoreflectance," Nat. Commun., **4**(1), p. 1640.

[129] Mukhopadhyay, S., Parker, D. S., Sales, B. C., Puretzky, A. A., McGuire, M. A., and Lindsay, L., 2018, "Two-Channel Model for Ultralow Thermal Conductivity of Crystalline Tl$_3$ VSe$_4$," Science, **360**(6396), pp. 1455–1458.

[130] Isaeva, L., Barbalinardo, G., Donadio, D., and Baroni, S., 2019, "Modeling Heat Transport in Crystals and Glasses From a Unified Lattice-Dynamical Approach," Nat. Commun., **10**(1), p. 3853.

[131] Simoncelli, M., Mauri, F., and Marzari, N., 2023, "Thermal Conductivity of Glasses: First-Principles Theory and Applications," NPJ Comput. Mater., **9**(1), p. 106.

[132] Rongione, N. A., Li, M., Wu, H., Nguyen, H. D., Kang, J. S., Ouyang, B., Xia, H., and Hu, Y., 2019, "High-Performance Solution-Processable Flexible SnSe Nanosheet Films for Lower Grade Waste Heat Recovery," Adv. Electron. Mater., **5**(3), p. 1800774.

[133] Li, M., Qin, Z., Cui, Y., Yang, C., Deng, C., Wang, Y., Kang, J. S., Xia, H., and Hu, Y., 2019, "Ultralight and Flexible Monolithic Polymer Aerogel With Extraordinary Thermal Insulation by A Facile Ambient Process," Adv. Mater. Interfaces, **6**, p. 1900314.

[134] Qin, Z., Li, M., Flohn, J., and Hu, Y., 2021, "Thermal Management Materials for Energy-Efficient and Sustainable Future Buildings," Chem. Commun., **57**(92), pp. 12236–12253.

[135] Maldovan, M., 2015, "Phonon Wave Interference and Thermal Bandgap Materials," Nat. Mater., **14**(7), pp. 667–674.

[136] Chen, G., Neagu, M., and Borca-Tasciuc, T., 1997, "Thermal Conductivity and Heat Transfer in Superlattices," MRS Proc., **478**, p. 85.

[137] Chen, G., 1998, "Thermal Conductivity and Ballistic-Phonon Transport in the Cross-Plane Direction of Superlattices," Phys. Rev. B, **57**(23), pp. 14958–14973.

[138] Hyldgaard, P., and Mahan, G. D., 1997, "Phonon Superlattice Transport," Phys. Rev. B, **56**(17), pp. 10754–10757.

[139] Tamura, S., Tanaka, Y., and Maris, H. J., 1999, "Phonon Group Velocity and Thermal Conduction in Superlattices," Phys. Rev. B, **60**(4), pp. 2627–2630.

[140] Kiselev, A. A., Kim, K. W., and Stroscio, M. A., 2000, "Thermal Conductivity of Si/Ge Superlattices: A Realistic Model With a Diatomic Unit Cell," Phys. Rev. B, **62**(11), pp. 6896–6899.

[141] Simkin, M. V., and Mahan, G. D., 2000, "Minimum Thermal Conductivity of Superlattices," Phys. Rev. Lett., **84**(5), pp. 927–930.

[142] Ravichandran, J., Yadav, A. K., Cheaito, R., Rossen, P. B., Soukiassian, A., Suresha, S. J., Duda, J. C., et al., 2014, "Crossover From Incoherent to Coherent Phonon Scattering in Epitaxial Oxide Superlattices," Nat. Mater., **13**(2), pp. 168–172.

[143] Garg, J., and Chen, G., 2013, "Minimum Thermal Conductivity in Superlattices: A First-Principles Formalism," Phys. Rev. B, **87**(14), p. 140302.

[144] Tian, Z., Esfarjani, K., and Chen, G., 2014, "Green's Function Studies of Phonon Transport Across Si/Ge Superlattices," Phys. Rev. B, **89**(23), p. 235307.

[145] Qiu, B., Chen, G., and Tian, Z., 2015, "Effects of Aperiodicity and Roughness on Coherent Heat Conduction in Superlattices," Nanoscale Microscale Thermophys. Eng., **19**(4), pp. 272–278.

[146] Landry, E. S., and McGaughey, A. J. H., 2009, "Effect of Interfacial Species Mixing on Phonon Transport in Semiconductor Superlattices," Phys. Rev. B, **79**(7), p. 075316.

[147] Latour, B., Volz, S., and Chalopin, Y., 2014, "Microscopic Description of Thermal-Phonon Coherence: From Coherent Transport to Diffuse Interface Scattering in Superlattices," Phys. Rev. B, **90**(1), p. 014307.

[148] Jain, A., Yu, Y.-J., and McGaughey, A. J. H., 2013, "Phonon Transport in Periodic Silicon Nanoporous Films With Feature Sizes Greater Than 100 nm," Phys. Rev. B, **87**(19), p. 195301.

[149] Mu, X., Zhang, T., Go, D. B., and Luo, T., 2015, "Coherent and Incoherent Phonon Thermal Transport in Isotopically Modified Graphene Superlattices," Carbon, **83**, pp. 208–216.

[150] Guo, R., Jho, Y.-D., and Minnich, A. J., 2018, "Coherent Control of Thermal Phonon Transport in Van Der Waals Superlattices," Nanoscale, **10**(30), pp. 14432–14440.

[151] Qu, X., and Gu, J., 2020, "Phonon Transport and Thermal Conductivity of Diamond Superlattice Nanowires: A Comparative Study With SiGe Superlattice Nanowires," RSC Adv., **10**(3), pp. 1243–1248.

[152] Lee, S.-M., Cahill, D. G., and Venkatasubramanian, R., 1997, "Thermal Conductivity of Si–Ge Superlattices," Appl. Phys. Lett., **70**(22), pp. 2957–2959.

[153] Luckyanova, M. N., Garg, J., Esfarjani, K., Jandl, A., Bulsara, M. T., Schmidt, A. J., Minnich, A. J., et al., 2012, "Coherent Phonon Heat Conduction in Superlattices," Science, **338**(6109), pp. 936–939.

[154] Christodoulides, A. D., Guo, P., Dai, L., Hoffman, J. M., Li, X., Zuo, X., Rosenmann, D., et al., 2021, "Signatures of Coherent Phonon Transport in Ultralow Thermal Conductivity Two-Dimensional Ruddlesden–Popper Phase Perovskites," ACS Nano, **15**(3), pp. 4165–4172.

[155] Zen, N., Puurtinen, T. A., Isotalo, T. J., Chaudhuri, S., and Maasilta, I. J., 2014, "Engineering Thermal Conductance Using a Two-Dimensional Phononic Crystal," Nat. Commun., **5**(1), p. 3435.

[156] Wingert, M. C., Chen, Z. C. Y., Dechaumphai, E., Moon, J., Kim, J.-H., Xiang, J., and Chen, R., 2011, "Thermal Conductivity of Ge and Ge–Si Core–Shell Nanowires in the Phonon Confinement Regime," Nano Lett., **11**(12), pp. 5507–5513.

[157] Poyser, C. L., Czerniuk, T., Akimov, A., Diroll, B. T., Gaulding, E. A., Salasyuk, A. S., Kent, A. J., Yakovlev, D. R., Bayer, M., and Murray, C. B., 2016, "Coherent Acoustic Phonons in Colloidal Semiconductor Nanocrystal Superlattices," ACS Nano, **10**(1), pp. 1163–1169.

[158] Venkatasubramanian, R., 2000, "Lattice Thermal Conductivity Reduction and Phonon Localizationlike Behavior in Superlattice Structures," Phys. Rev. B, **61**(4), pp. 3091–3097.

[159] Wang, Y., Huang, H., and Ruan, X., 2014, "Decomposition of Coherent and Incoherent Phonon Conduction in Superlattices and Random Multilayers," Phys. Rev. B, **90**(16), p. 165406.

[160] Nika, D. L., Cocemasov, A. I., Crismari, D. V., and Balandin, A. A., 2013, "Thermal Conductivity Inhibition in Phonon Engineered Core-Shell Cross-Section Modulated Si/Ge Nanowires," Appl. Phys. Lett., **102**, p. 213109.

[161] Mendoza, J., and Chen, G., 2016, "Anderson Localization of Thermal Phonons Leads to a Thermal Conductivity Maximum," Nano Lett, **16**(12), pp. 7616–7620.

[162] Luckyanova, M. N., Mendoza, J., Lu, H., Song, B., Huang, S., Zhou, J., Li, M., et al., 2018, "Phonon Localization in Heat Conduction," Sci. Adv., **4**(12), p. eaat9460.

[163] Hu, R., Iwamoto, S., Feng, L., Ju, S., Hu, S., Ohnishi, M., Nagai, N., Hirakawa, K., and Shiomi, J., 2020, "Machine-Learning-Optimized Aperiodic Superlattice Minimizes Coherent Phonon Heat Conduction," Phys. Rev. X, **10**(2), p. 021050.

[164] Roy Chowdhury, P., Reynolds, C., Garrett, A., Feng, T., Adiga, S. P., and Ruan, X., 2020, "Machine Learning Maximized Anderson Localization of Phonons in Aperiodic Superlattices," Nano Energy, **69**, p. 104428.

[165] Wilson, R. B., and Cahill, D. G., 2012, "Experimental Validation of the Interfacial Form of the Wiedemann-Franz Law," Phys. Rev. Lett., **108**(25), p. 255901.

[166] Lyeo, H.-K., and Cahill, D. G., 2006, "Thermal Conductance of Interfaces Between Highly Dissimilar Materials," Phys. Rev. B—Condens. Matter Mater. Phys., **73**(14), p. 144301.

[167] Monachon, C., Weber, L., and Dames, C., 2016, "Thermal Boundary Conductance: A Materials Science Perspective," Annu. Rev. Mater. Res., **46**(1), pp. 433–463.

[168] Li, M., Pan, K., Ge, Y., Huynh, K., Goorsky, M. S., Fisher, T. S., and Hu, Y., 2024, "Wafer-Scale Bonded GaN–AlN With High Interface Thermal Conductance," Appl. Phys. Lett., **125**(3), p. 032104.

[169] Adnan, K. Z., and Feng, T., 2024, "Thermal Boundary Conductance and Thermal Conductivity Strongly Depend on Nearby Environment," Phys. Rev. B, **109**(24), p. 245302.

[170] Swartz, E. T., and Pohl, R. O., 1989, "Thermal Boundary Resistance," Rev. Mod. Phys., **61**(3), pp. 605–668.

[171] Sadasivam, S., Che, Y., Huang, Z., Chen, L., Kumar, S., and Fisher, T. S., 2014, "The Atomistic Green's Function Method for Interfacial Phonon Transport," Annu. Rev. Heat Transfer, **17**, pp. 89–145.

[172] Young, D. A., and Maris, H. J., 1989, "Lattice-Dynamical Calculation of the Kapitza Resistance Between FCC Lattices," Phys. Rev. B, **40**(6), pp. 3685–3693.

[173] Zhao, H., and Freund, J. B., 2005, "Lattice-Dynamical Calculation of Phonon Scattering at Ideal Si–Ge Interfaces," J. Appl. Phys., **97**(2), p. 024903.

[174] Yang, H.-A., and Cao, B.-Y., 2023, "Mode-Resolved Phonon Transmittance Using Lattice Dynamics: Robust Algorithm and Statistical Characteristics," J. Appl. Phys., **134**(15), p. 155302.

[175] van Duin, A. C. T., Dasgupta, S., Lorant, F., and Goddard, W., 2001, "A. ReaxFF: A Reactive Force Field for Hydrocarbons," J. Phys. Chem. A, **105**(41), pp. 9396–9409.

[176] Deringer, V. L., Caro, M. A., and Csányi, G., 2019, "Machine Learning Interatomic Potentials as Emerging Tools for Materials Science," Adv. Mater., **31**(46), p. 1902765.

[177] Mueller, T., Hernandez, A., and Wang, C., 2020, "Machine Learning for Interatomic Potential Models," J. Chem. Phys., **152**(5), p. 050902.

[178] Pollack, G. L., 1969, "Kapitza resistance," Rev. Mod. Phys., **41**(1), pp. 48–81.

[179] Zhang, X., Fujiwara, S., and Fujii, M., 2000, "Measurements of Thermal Conductivity and Electrical Conductivity of a Single Carbon Fiber," Int. J. Thermophys., **21**, pp. 965–980.

[180] Fujii, M., Zhang, X., Xie, H., Ago, H., Takahashi, K., Ikuta, T., Abe, H., and Shimizu, T., 2005, "Measuring the Thermal Conductivity of a Single Carbon Nanotube," Phys. Rev. Lett., **95**(6), p. 065502.

[181] Hirotani, J., Ikuta, T., Nishiyama, T., and Takahashi, K., 2011, "Thermal Boundary Resistance Between the End of an Individual Carbon Nanotube and a Au Surface," Nanotechnology, **22**(31), p. 315702.

[182] Lee, S.-M., and Cahill, D. G., 1997, "Heat Transport in Thin Dielectric Films," J. Appl. Phys., **81**(6), pp. 2590–2595.

[183] Chen, Z., Jang, W., Bao, W., Lau, C. N., and Dames, C., 2009, "Thermal Contact Resistance Between Graphene and Silicon Dioxide," Appl. Phys. Lett., **95**(16), p. 161910.

[184] Dames, C., 2013, "Measuring the Thermal Conductivity of Thin Films: 3 Omega and Related Electrothermal Methods," Annu. Rev. Heat Transfer, **16**(1), pp. 7–49.

[185] Malen, J. A., Baheti, K., Tong, T., Zhao, Y., Hudgings, J. A., and Majumdar, A., 2011, "Optical Measurement of Thermal Conductivity Using Fiber Aligned Frequency Domain Thermoreflectance," ASME J. Heat Mass Transfer-Trans. ASME, **133**(8), p. 081601.

[186] Koh, Y. K., Bae, M.-H., Cahill, D. G., and Pop, E., 2010, "Heat Conduction Across Monolayer and Few-Layer Graphenes," Nano Lett., **10**(11), pp. 4363–4368.

[187] Brown, D. B., Shen, W., Li, X., Xiao, K., Geohegan, D. B., and Kumar, S., 2019, "Spatial Mapping of Thermal Boundary Conductance at Metal–Molybdenum Diselenide Interfaces," ACS Appl. Mater. Interfaces, **11**(15), pp. 14418–14426.

[188] Song, B., Fiorino, A., Meyhofer, E., and Reddy, P., 2015, "Near-Field Radiative Thermal Transport: From Theory to Experiment," AIP Adv., **5**, p. 53503.

[189] Polder, D., and Van Hove, M., 1971, "Theory of Radiative Heat Transfer Between Closely Spaced Bodies," Phys. Rev. B, **4**(10), pp. 3303–3314.

[190] Rytov, S. M., and Erkku, H., 1959, *Theory of Electric Fluctuations and Thermal Radiation*, Air Force Cambridge Research Center, Bedford, MA.

[191] Mulet, J.-P., Joulain, K., Carminati, R., and Greffet, J.-J., 2001, "Nanoscale Radiative Heat Transfer Between a Small Particle and a Plane Surface," Appl. Phys. Lett., **78**(19), pp. 2931–2933.

[192] Narayanaswamy, A., Shen, S., and Chen, G., 2008, "Near-Field Radiative Heat Transfer Between a Sphere and a Substrate," Phys. Rev. B, **78**(11), p. 115303.

[193] Cravalho, E. G., Tien, C. L., and Caren, R. P., 1967, "Effect of Small Spacings on Radiative Transfer Between Two Dielectrics," ASME J. Heat Mass Transfer-Trans. ASME, **89**(4), pp. 351–358.

[194] Domoto, G. A., Boehm, R. F., and Tien, C. L., 1970, "Experimental Investigation of Radiative Transfer Between Metallic Surfaces at Cryogenic Temperatures," ASME J. Heat Mass Transfer-Trans. ASME, **92**(3), pp. 412–416.

[195] Hargreaves, C. M., 1969, "Anomalous Radiative Transfer Between Closely-Spaced Bodies," Phys. Lett. A, **30**(9), pp. 491–492.

[196] Xu, J.-B., Läuger, K., Möller, R., Dransfeld, K., and Wilson, I. H., 1994, "Heat Transfer Between Two Metallic Surfaces at Small Distances," J. Appl. Phys., **76**(11), pp. 7209–7216.

[197] Kittel, A., Müller-Hirsch, W., Parisi, J., Biehs, S.-A., Reddig, D., and Holthaus, M., 2005, "Near-Field Heat Transfer in a Scanning Thermal Microscope," Phys. Rev. Lett., **95**(22), p. 224301.

[198] Hu, L., Narayanaswamy, A., Chen, X., and Chen, G., 2008, "Near-Field Thermal Radiation Between Two Closely Spaced Glass Plates Exceeding Planck's Blackbody Radiation Law," Appl. Phys. Lett., **92**(13), p. 133106.

[199] Varesi, J., Lai, J., Perazzo, T., Shi, Z., and Majumdar, A., 1997, "Photothermal Measurements at Picowatt Resolution Using Uncooled Micro-Optomechanical Sensors," Appl. Phys. Lett., **71**(3), pp. 306–308.

[200] Luo, T., and Chen, G., 2013, "Nanoscale Heat Transfer – From Computation to Experiment," Phys. Chem. Chem. Phys., **15**(10), p. 3389.

[201] Gimzewski, J. K., Gerber, C., Meyer, E., and Schlittler, R. R., 1994, "Observation of a Chemical Reaction Using a Micromechanical Sensor," Chem. Phys. Lett., **217**(5–6), pp. 589–594.

[202] Mohideen, U., and Roy, A., 1998, "Precision Measurement of the Casimir Force From 0.1 to 0.9 μm," Phys. Rev. Lett., **81**(21), pp. 4549–4552.

[203] Rousseau, E., Siria, A., Jourdan, G., Volz, S., Comin, F., Chevrier, J., and Greffet, J.-J., 2009, "Radiative Heat Transfer at the Nanoscale," Nat. Photonics, **3**(9), pp. 514–517.

[204] Shen, S., Narayanaswamy, A., and Chen, G., 2009, "Surface Phonon Polaritons Mediated Energy Transfer Between Nanoscale Gaps," Nano Lett., **9**(8), pp. 2909–2913.

[205] Messina, R., and Antezza, M., 2011, "Scattering-Matrix Approach to Casimir-Lifshitz Force and Heat Transfer Out of Thermal Equilibrium Between Arbitrary Bodies," Phys. Rev. A, **84**(4), p. 042102.

[206] Krüger, M., Emig, T., and Kardar, M., 2011, "Nonequilibrium Electromagnetic Fluctuations: Heat Transfer and Interactions," Phys. Rev. Lett., **106**(21), p. 210404.

[207] Krüger, M., Bimonte, G., Emig, T., and Kardar, M., 2012, "Trace Formulas for Nonequilibrium Casimir Interactions, Heat Radiation, and Heat Transfer for Arbitrary Objects," Phys. Rev. B, **86**(11), p. 115423.

[208] Rodriguez, A. W., Reid, M. T. H., and Johnson, S. G., 2012, "Fluctuating-Surface-Current Formulation of Radiative Heat Transfer for Arbitrary Geometries," Phys. Rev. B, **86**(22), p. 220302.

[209] Rodriguez, A. W., Reid, M. T. H., and Johnson, S. G., 2013, "Fluctuating-Surface-Current Formulation of Radiative Heat Transfer: Theory and Applications," Phys. Rev. B, **88**(5), p. 054305.

[210] Rodriguez, A. W., Reid, M. T. H., Varela, J., Joannopoulos, J. D., Capasso, F., and Johnson, S. G., 2013, "Anomalous Near-Field Heat Transfer Between a Cylinder and a Perforated Surface," Phys. Rev. Lett., **110**(1), p. 014301.

[211] Luo, C., Narayanaswamy, A., Chen, G., and Joannopoulos, J. D., 2004, "Thermal Radiation From Photonic Crystals: A Direct Calculation," Phys Rev Lett, **93**(21), p. 213905.

[212] Otey, C. R., Zhu, L., Sandhu, S., and Fan, S., 2014, "Fluctuational Electrodynamics Calculations of Near-Field Heat Transfer in Non-Planar Geometries: A Brief Overview," J. Quant. Spectrosc. Radiat. Transfer, **132**, pp. 3–11.

[213] Narayanaswamy, A., and Chen, G., 2003, "Surface Modes for Near Field Thermophotovoltaics," Appl. Phys. Lett., **82**(20), pp. 3544–3546.

[214] Biehs, S.-A., Rosa, F. S. S., and Ben-Abdallah, P., 2011, "Modulation of Near-Field Heat Transfer Between Two Gratings," Appl. Phys. Lett., **98**, p. 243102.

[215] Huang, Y., Boriskina, S. V., and Chen, G., 2014, "Electrically Tunable Near-Field Radiative Heat Transfer Via Ferroelectric Materials," Appl. Phys. Lett., **105**(24), p. 244102.

[216] Otey, C. R., Lau, W. T., and Fan, S., 2010, "Thermal Rectification Through Vacuum," Phys. Rev. Lett., **104**(15), p. 154301.

[217] Basu, S., and Francoeur, M., 2011, "Near-Field Radiative Transfer Based Thermal Rectification Using Doped Silicon," Appl. Phys. Lett., **98**(11), p. 113106.

[218] Ben-Abdallah, P., and Biehs, S.-A., 2014, "Near-Field Thermal Transistor," Phys. Rev. Lett., **112**(4), p. 044301.

[219] Mills, D. L., 1975, "Attenuation of Surface Polaritons by Surface Roughness," Phys. Rev. B, **12**(10), pp. 4036–4046.

[220] Schoenwald, J., Burstein, E., and Elson, J. M., 1993, "Propagation of Surface Polaritons Over Macroscopic Distances at Optical Frequencies," Solid State Commun., **88**(11–12), pp. 1067–1071.

[221] Yang, F., Sambles, J. R., and Bradberry, G. W., 1991, "Long-Range Surface Modes Supported by Thin Films," Phys. Rev. B, **44**(11), pp. 5855–5872.

[222] Chen, D.-Z. A., Narayanaswamy, A., and Chen, G., 2005, "Surface Phonon-Polariton Mediated Thermal Conductivity Enhancement of Amorphous Thin Films," Phys. Rev. B, **72**(15), p. 155435.

[223] Ordonez-Miranda, J., Tranchant, L., Tokunaga, T., Kim, B., Palpant, B., Chalopin, Y., Antoni, T., and Volz, S., 2013, "Anomalous Thermal Conductivity by Surface Phonon-Polaritons of Polar Nano Thin Films Due to Their Asymmetric Surrounding Media," J. Appl. Phys., **113**(8), p. 084311.

[224] Ordonez-Miranda, J., Tranchant, L., Kim, B., Chalopin, Y., Antoni, T., and Volz, S., 2014, "Quantized Thermal Conductance of Nanowires at Room Temperature Due to Zenneck Surface-Phonon Polaritons," Phys. Rev. Lett., **112**(5), p. 055901.

[225] Ordonez-Miranda, J., Tranchant, L., Joulain, K., Ezzahri, Y., Drevillon, J., and Volz, S., 2016, "Thermal Energy Transport in a Surface Phonon-Polariton Crystal," Phys. Rev. B, **93**(3), p. 035428.

[226] Yun, K. H., Lee, B. J., and Lee, S. H., 2022, "Modeling Effective Thermal Conductivity Enhanced by Surface Waves Using the Boltzmann Transport Equation," Sci. Rep., **12**(1), p. 15477.

[227] Chen, D.-Z. A., and Chen, G., 2007, "Measurement of Silicon Dioxide Surface Phonon-Polariton Propagation Length by Attenuated Total Reflection," Appl. Phys. Lett., **91**(12), p. 121906.

[228] Tranchant, L., Hamamura, S., Ordonez-Miranda, J., Yabuki, T., Vega-Flick, A., Cervantes-Alvarez, F., Alvarado-Gil, J. J., Volz, S., and Miyazaki, K., 2019, "Two-Dimensional Phonon Polariton Heat Transport," Nano Lett., **19**(10), pp. 6924–6930.

[229] Wu, Y., Ordonez-Miranda, J., Gluchko, S., Anufriev, R., Meneses, D. D. S., Del Campo, L., Volz, S., and Nomura, M., 2020, "Enhanced Thermal Conduction by Surface Phonon-Polaritons," Sci. Adv., **6**(40), p. eabb4461.

[230] Wu, Y., Ordonez-Miranda, J., Jalabert, L., Tachikawa, S., Anufriev, R., Fujita, H., Volz, S., and Nomura, M., 2022, "Observation of Heat Transport Mediated by the Propagation Distance of Surface Phonon-Polaritons Over Hundreds of Micrometers," Appl. Phys. Lett., **121**(11), p. 112203.

[231] Pei, Y., Chen, L., Jeon, W., Liu, Z., and Chen, R., 2023, "Low-Dimensional Heat Conduction in Surface Phonon Polariton Waveguide," Nat. Commun., **14**(1), p. 8242.

[232] Pan, Z., Lu, G., Li, X., McBride, J. R., Juneja, R., Long, M., Lindsay, L., Caldwell, J. D., and Li, D., 2023, "Remarkable Heat Conduction Mediated by Non-Equilibrium Phonon Polaritons," Nature, **623**(7986), pp. 307–312.

[233] Li, M., Dai, L., and Hu, Y., 2022, "Machine Learning for Harnessing Thermal Energy: From Materials Discovery to System Optimization," ACS Energy Lett., **7**(10), pp. 3204–3226.

[234] Zhang, L., and Niu, Q., 2015, "Chiral Phonons at High-Symmetry Points in Monolayer Hexagonal Lattices," Phys. Rev. Lett., **115**(11), p. 115502.

[235] Zhu, H., Yi, J., Li, M.-Y., Xiao, J., Zhang, L., Yang, C.-W., Kaindl, R. A., Li, L.-J., Wang, Y., and Zhang, X., 2018, "Observation of Chiral Phonons," Science, **359**(6375), pp. 579–582.

[236] Baydin, A., Hernandez, F. G. G., Rodriguez-Vega, M., Okazaki, A. K., Tay, F., Noe, G. T., Katayama, I., et al., 2022, "Magnetic Control of Soft Chiral Phonons in PbTe," Phys. Rev. Lett., **128**(7), p. 075901.

[237] Süsstrunk, R., and Huber, S. D., 2016, "Classification of Topological Phonons in Linear Mechanical Metamaterials," Proc. Natl. Acad. Sci., **113**(33), pp. E4767–E4775.

[238] Anirban, A., 2024, "Topological Phonons in Graphene," Nat. Rev. Phys., **6**, p. 81.

[239] Xu, Y., Vergniory, M. G., Ma, D.-S., Mañes, J. L., Song, Z.-D., Bernevig, B. A., Regnault, N., and Elcoro, L., 2024, "Catalog of Topological Phonon Materials," Science, **384**(6696), p. eadf8458.